nature cancer

ARTICLES

https://doi.org/10.1038/s43018-020-0064-0

Check for updates

Activation of p38α stress-activated protein kinase drives the formation of the pre-metastatic niche in the lungs

Jun Gui[1], Farima Zahedi[1], Angelica Ortiz[1], Christina Cho[1], Kanstantsin V. Katlinski[1], Kevin Alicea-Torres[2], Jinyang Li[3], Leslie Todd[1], Hongru Zhang[1], Daniel P. Beiting[4], Cindy Sander[5], John M. Kirkwood[5], Bryan E. Snow[6], Andrew C. Wakeham[6], Tak W. Mak[6], J. Alan Diehl[7], Constantinos Koumenis[8], Sandra W. Ryeom[9], Ben Z. Stanger[3], Ellen Puré[1], Dmitry I. Gabrilovich[2] and Serge Y. Fuchs[1]✉

Primary tumor-derived factors act upon normal cells to generate a pre-metastatic niche, which promotes colonization of target organs by disseminated malignant cells. Here we report that tumor-derived factor-induced activation of the p38α kinase in lung fibroblasts plays a critical role in the formation of a pre-metastatic niche in the lungs and subsequent pulmonary metastases. Activation of p38α led to inactivation of type I interferon signaling and stimulation of expression of fibroblast activation protein. Fibroblast activation protein played a key role in remodeling of the extracellular matrix as well as inducing the expression of chemokines that enable lung infiltration by neutrophils. Increased activity of p38 in normal cells was associated with metastatic disease and poor prognosis in human patients with melanoma, whereas inactivation of p38 suppressed lung metastases. We discuss the p38α-driven mechanisms stimulating the metastatic processes and potential use of p38 inhibitors in adjuvant therapy of metastatic cancers.

Malignant cells secrete membranous vesicles and soluble factors that target normal cells in the bone marrow and peripheral tissues to generate pre-metastatic niches in the target organs. These niches provide a beacon and a safe haven for circulating tumor cells, enabling their homing and subsequent metastatic colonization[1–4].

Lungs are a primary site for hematogenous metastasis of many malignant tumors[5,6]. Many tumor-derived soluble factors[3,7] and extracellular vesicles[3,8,9] act upon bone marrow-derived and lung cells, resulting in a lung myeloid infiltration, expression of specific inflammatory genes (for example, *S100a8/9*) and a localized stromagenic switch, exemplified by the activation of lung fibroblasts and ensuing extracellular matrix remodeling events (for example, accumulation of fibronectin)[1,4,10]. These common elements of pre-metastatic niches provide favorable conditions for proliferation and survival of disseminated malignant cells, leading to metastatic colonization[1,4,11].

The pro-metastatic secretome of primary tumors contains a multitude of factors, which activate a variety of sensors on different types of normal cells in the bone marrow and lung leading to the generation of pre-metastatic niches[2,9]. Despite such mechanistic diversity, these pathways converge to evoke the equivalent phenotypic manifestations of a pulmonary niche[1,4,11]. These commonalities suggest that numerous stimuli act through many sensors to trigger a common pathway underlying the generation of the niche. Here we sought to identify and characterize such signaling events activated by tumor-derived factors (TDFs) that act upon healthy cells to promote the formation of a pre-metastatic niche in the lungs.

Many danger-associated molecular patterns and inflammatory cytokines generated by malignant cells activate the p38 stress-activated protein kinases[12]. Among α/β/γ/δ isoforms of this subfamily, p38α, encoded by the *MAPK14* gene, is ubiquitously expressed[12]. p38α phosphorylates numerous important substrates (for example, ATF2, CHOP, CREB and so on) and plays a key role in many homeostatic functions and in the pathogenesis of inflammation and cancer[13–15]. Activation of p38α by melanoma TDFs downregulates the IFNAR1 chain of type I interferon (IFN) receptor[16], which otherwise acts to suppress distant metastases in mouse melanoma models[17,18].

Here we report that TDFs from metastatic malignant cells activate p38α in lung fibroblasts and trigger a sequence of downstream intracellular events, including downregulation of IFNAR1 and ensuing induction of the fibroblast activation protein (FAP, which is implicated in many aspects of tumorigenesis[19–21]). FAP expression and its protease activity are, in turn, required for accumulation of lung fibronectin and induction of CXCL1-like chemokines and recruitment of neutrophils. These events generate favorable conditions for metastatic pulmonary colonization. Whereas activation of p38α in normal cells from patients with melanoma correlates with increased metastatic disease and poor prognosis, use of p38 inhibitors in the context of adjuvant therapy notably decreases lung

[1]Department of Biomedical Sciences, School of Veterinary Medicine, University of Pennsylvania, Philadelphia, PA, USA. [2]Immunology, Microenvironment, and Metastasis Program, Wistar Institute, Philadelphia, PA, USA. [3]Department of Medicine, Perelman School of Medicine, University of Pennsylvania, Philadelphia, PA, USA. [4]Department of Pathobiology, School of Veterinary Medicine, University of Pennsylvania, Philadelphia, PA, USA. [5]Department of Medicine, University of Pittsburgh School of Medicine, Pittsburgh, PA, USA. [6]The Campbell Family Institute for Breast Cancer Research, Princess Margaret Cancer Centre, University Health Network, Toronto, Ontario, Canada. [7]Department of Biochemistry, Case Western Reserve University School of Medicine, Cleveland, OH, USA. [8]Department of Radiation Oncology, Perelman School of Medicine, University of Pennsylvania, Philadelphia, PA, USA. [9]Department of Cancer Biology, Perelman School of Medicine, University of Pennsylvania, Philadelphia, PA, USA. ✉e-mail: syfuchs@upenn.edu

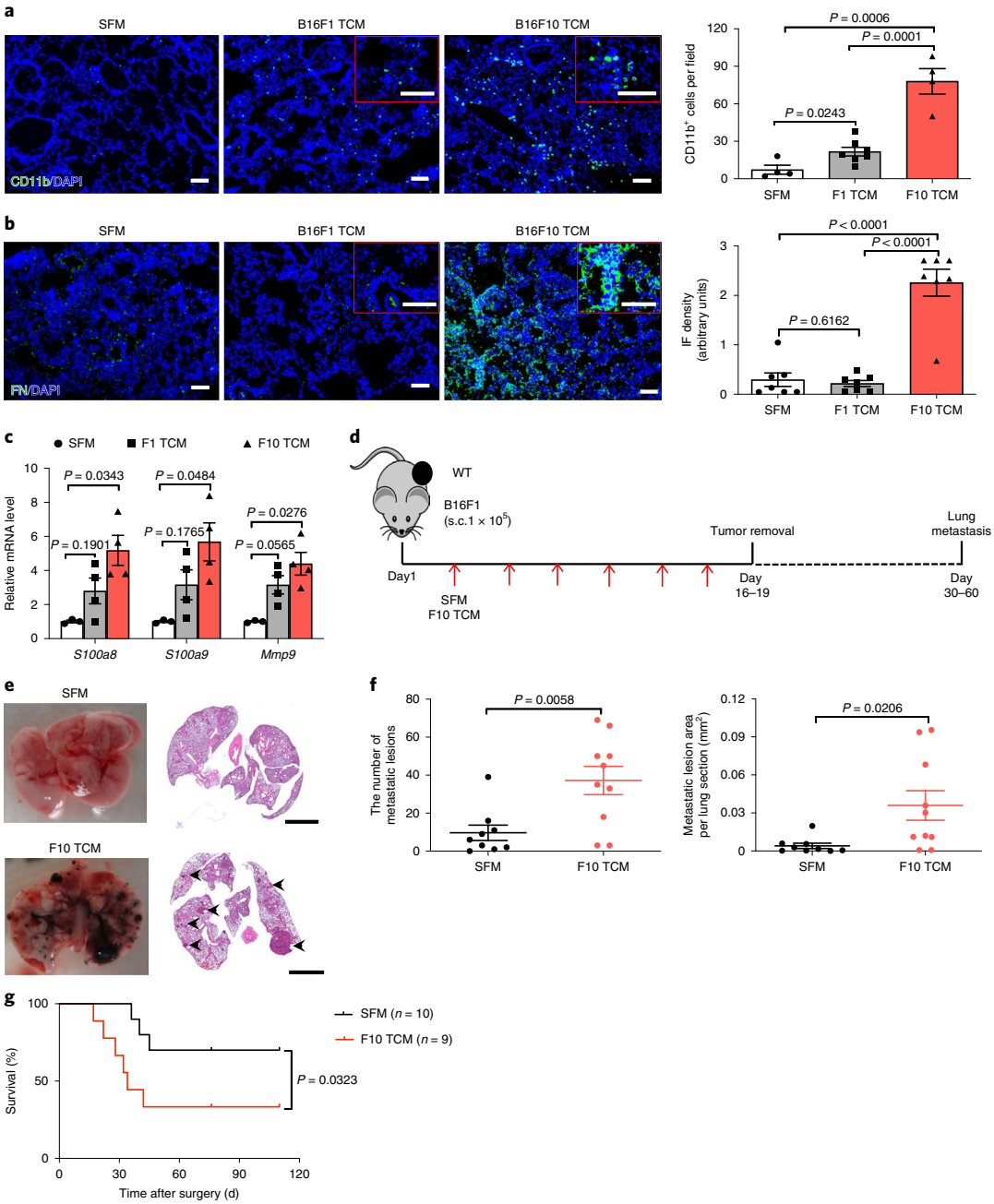

Fig. 1 | TDFs from highly metastatic melanoma cells induce the pre-metastatic niche and stimulate pulmonary metastases. a, A representative immunofluorescence staining of CD11b (left) and quantification of CD11b$^+$ cells (right) in the lung tissues from WT mice treated with tumor-conditioned media (TCM) from B16F1 or B16F10 cells, or with serum-free media (SFM) as control (100 µl intravenously (i.v.), 3x per week for 3 weeks). Quantitative data are shown as mean ± s.e.m. ($n = 4$ mice for SFM and F10 TCM groups, $n = 7$ mice for F1 TCM group). Two-tailed unpaired *t*-test was performed for the comparisons between two groups. Here and henceforth, the inset shows a zoomed (×2) area of the stained image. Scale bar, 100 µm. **b**, A representative immunofluorescence staining of fibronectin (left) and the quantification of fibronectin level (right) in the lung tissues from WT mice treated with B16F1 TCM, or B16F10 TCM or SFM as control (100 µl i.v., 3x per week for 3 weeks). Scale bar, 100 µm. Quantitative data are shown as mean ± s.e.m. ($n = 7$ mice per group). Two-tailed unpaired *t*-test was performed for the comparisons between two groups. **c**, Quantitative PCR (qPCR) analysis of mRNA levels of the niche genes in the lung tissues from WT mice treated with B16F1 TCM, or B16F10 TCM or SFM as control (100 µl i.v., 3x per week for 3 weeks). Data are shown as mean ± s.e.m. ($n = 3$ mice for SFM group, $n = 4$ mice for F1 TCM and F10 TCM groups). Two-way ANOVA and Tukey's multiple comparisons test were performed. **d**, Schematic illustration for analysis of the lung metastasis in the B16F1 tumor-bearing mice treated with SFM or B16F10 TCM (100 µl every other day until primary tumor removal upon reaching the size ~200 mm^2). **e**, Representative lung images and the corresponding H&E-stained lung sections in the B16F1 tumor-bearing mice treated with SFM or B16F10 TCM after surgery. Scale bar, 1 mm. Similar results were obtained from three independent experiments. **f**, Quantification of the number of metastatic lesions and total area in the lung tissue sections from B16F1 tumor-bearing mice treated with SFM ($n = 9$ mice) or B16F10 TCM ($n = 10$ mice) after surgery. Data are shown as mean ± s.e.m. Two-tailed unpaired *t*-test was performed. **g**, Kaplan–Meier analysis of survival of B16F1 tumor-bearing mice treated with SFM ($n = 10$ mice) or B16F10 TCM ($n = 9$ mice) after surgery by Gehan–Breslow–Wilcoxon test. F1, B16F1; F10, B16F10; IF, immunofluorescence; s.c., subcutaneously.

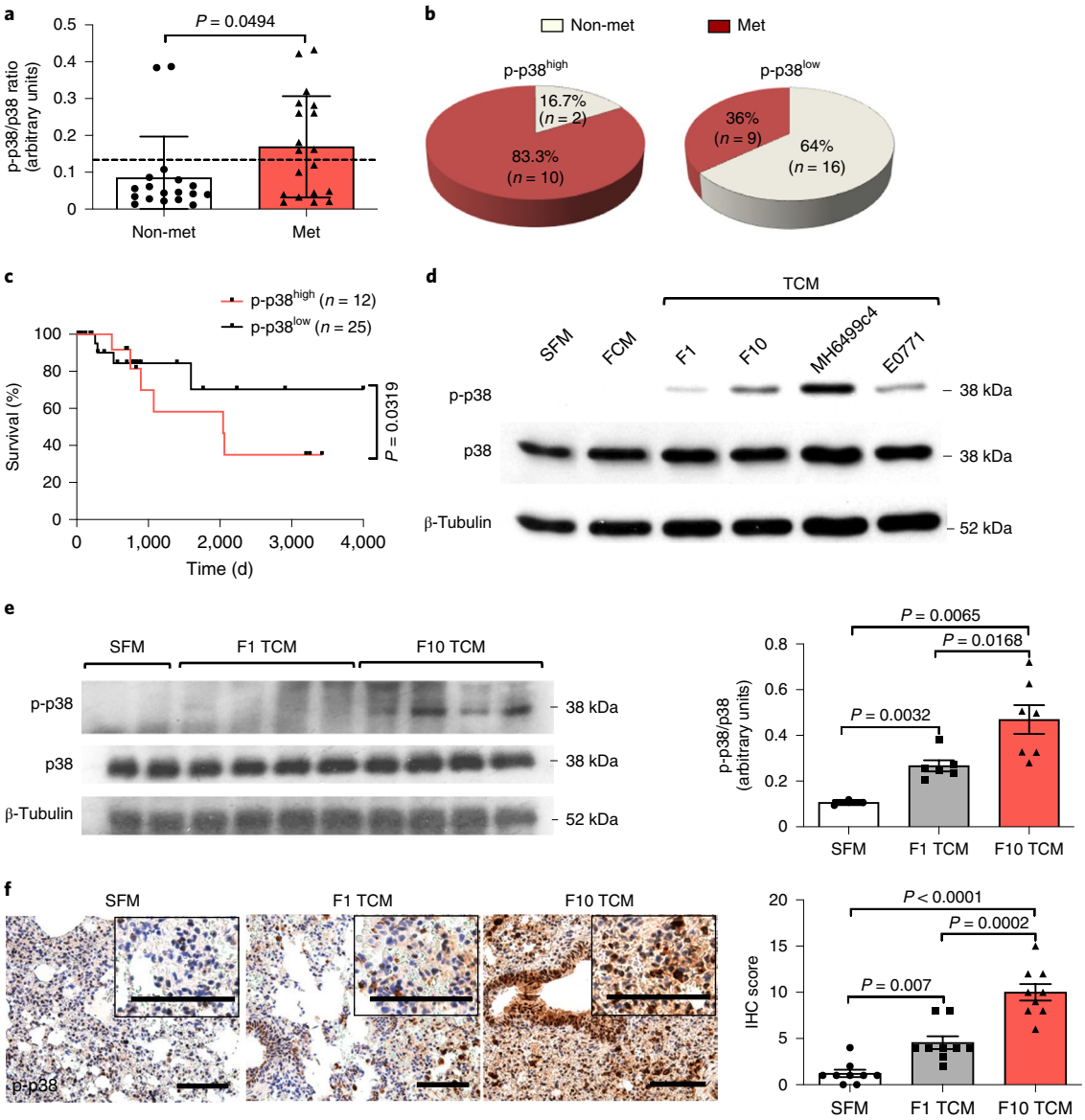

Fig. 2 | TDF-induced activation of p38 kinase correlates with metastatic disease in human patients with melanoma and mouse melanoma model. a, The phospho-p38 (p-p38)/total p38 ratio in the leukocytes isolated from the peripheral blood of patients with melanoma with metastasis ($n=19$) and without metastasis ($n=18$). The dashed line denotes the average p-p38/p38 ratio among all patients with melanoma. Data are shown as mean ± s.e.m. Two-tailed unpaired *t*-test was performed. **b**, Documented metastases in patients with melanoma whose lymphocytes had greater (p-p38/p38^{high}) or lower (p-p38/p38^{low}) levels of p-p38/p38 signal ratio compared with the average p-p38/p38 ratio among all patients with melanoma. Fisher's exact test was performed. $P=0.0128$. **c**, Kaplan–Meier analysis of survival of patients with melanoma classified as p-p38/p38^{high} ($n=12$) or p-p38/p38^{low} ($n=25$) by log-rank test. **d**, A representative western blot analysis of p-p38 and total p38 in the WT lung fibroblasts 1 h after SFM, conditioned medium from normal lung fibroblasts (FCM) or TCM from different malignant cells including B16F1 and B16F10 melanoma, MH6499c4 pancreatic ductal adenocarcinoma and E0771 mammary adenocarcinoma cell lines. Similar results were obtained from three independent experiments. **e**, A representative western blot analysis of p-p38/p38 (left) and quantification of the ratio of p-p38/p38 (right) in the lung tissue lysates isolated from WT mice treated with B16F1 TCM ($n=6$ mice), B16F10 TCM ($n=7$ mice) or SFM ($n=3$ mice) as control (100 µl i.v., 3x per week for 3 weeks). Quantitative data are shown as mean ± s.e.m. Two-tailed unpaired *t*-test was performed for the comparisons between two groups. **f**, A representative IHC staining of p-p38 (left) and quantification of IHC score for p-p38 (right) in the lung tissue sections from WT mice treated with B16F1 TCM, or B16F10 TCM or SFM as control (100 µl i.v., 3x per week for 3 weeks). Scale bar, 100 µm. Quantitative data are shown as mean ± s.e.m. ($n=9$ mice per group). Two-tailed unpaired *t*-test was performed for the comparisons between two groups. Met, patients with metastases; Non-met, patients without metastases.

metastases of mouse melanoma. In all, these results support a key role of p38α kinase in development of a pre-metastatic niche and metastatic lung colonization.

Results

TDFs from highly metastatic tumor cells activate p38 kinase and promote the p38-dependent generation of a pulmonary pre-metastatic niche. We sought to characterize the signaling pathways activated in normal cells by TDFs, which drive the generation of a pre-metastatic niche in the lungs. Given that lung metastases can be stimulated by both tumor-derived extracellular vesicles[8,9] and soluble molecules[7] that can be released by primary tumors into the systemic circulation, we administered into mice the entire cell culture media conditioned by syngeneic cancer

cells. Here we used B16 mouse melanoma-derived isogenic cell lines exhibiting high (B16F10) or low (B16F1) metastatic activity (characterized in ref. [22] and Extended Data Fig. 1a–c). Intravenous administration of B16F10 cell-conditioned media into wild-type (WT) mice led to a robust generation of a pre-metastatic niche in the lungs, manifested by myeloid infiltration (Fig. 1a), accumulation of fibronectin (Fig. 1b) and increased expression of *S100a8*, *S100a9* and *Mmp9* genes (Fig. 1c). Importantly, these changes were less pronounced in response to TDFs from less metastatic B16F1 cells (Fig. 1a–c).

To determine the importance of TDFs in the metastatic activities of malignant cells, we supplemented subcutaneous growth of B16F1 tumors with administration of highly metastatic B16F10-derived TDFs (Fig. 1d). Without accelerating growth of primary B16F1 tumors (Extended Data Fig. 1d), B16F10-derived TDFs increased the number and size of B16F1 lung metastases (Fig. 1e,f) and decreased animal survival (Fig. 1g). These results suggest that production of TDFs that can induce the generation of a pre-metastatic niche plays an important role in defining the metastatic potential of malignant cells.

Given that p38 kinase activity can be stimulated in response to cancer-cell-produced soluble factors (for example, TNFα and IL-1 (refs. [7,16])) or extracellular vesicles[18], we examined activation of p38 (assessed by its phosphorylation) in normal peripheral blood leukocytes isolated from patients with melanoma with or without metastatic disease (Extended Data Fig. 2a). Leukocytes from patients without signs of metastatic disease exhibited a notably lower level of p38 activation (Fig. 2a). Conversely, high levels of p38 activation were associated with occurrence of metastatic disease (Fig. 2b) and poor survival of these patients (Fig. 2c). These results suggest that human metastatic melanoma-derived TDFs activate p38 in normal cells and indirectly implicate this activation in the metastatic process.

Next we sought to re-capitulate these observations from human patients in mouse models. TDFs from highly metastatic melanoma and pancreatic or mammary adenocarcinoma cells activated p38 in primary mouse lung fibroblasts in vitro (Fig. 2d). We observed a greater activation of p38 in vitro or in the lung tissues of mice that received B16F10-derived factors compared with those from normal fibroblasts or less metastatic B16F1 melanoma cells (Fig. 2d–f). To determine whether TDFs activate pathways downstream of p38, we examined the expression of IFNAR1, which plays a role in limiting melanoma metastases[17,18] and was shown to be phosphorylated, ubiquitinated and downregulated in response to soluble or vesicular TDFs in a p38-dependent manner[16,18].

TDFs from metastatic pancreatic or mammary adenocarcinoma cells notably downregulated IFNAR1 in vitro (Extended Data Fig. 2b). In addition, TDFs from highly metastatic B16F10 (but not B16F1) cells significantly decreased IFNAR1 levels in vitro and in mouse lung tissues (Extended Data Fig. 2b,c). In line with these observations, a greater extent of lung metastatic lesions (Extended Data Fig. 2d,e) and poorer survival (Extended Data Fig. 2f) were observed in B16F1 tumor-bearing *Ifnar1*$^{-/-}$ mice compared with WT animals; these data further suggest an important role of IFNAR1 loss in metastatic disease.

Importantly, treatment of cells or mice with the p38 inhibitor ralimetinib (LY2228820) attenuated downregulation of IFNAR1 in vitro (Extended Data Fig. 3a) and in vivo (Fig. 3a). Ralimetinib also inhibited TDF-induced generation of a pulmonary pre-metastatic niche, manifested by myeloid infiltration (Fig. 3b), accumulation of fibronectin (Fig. 3c) and increased expression of *S100a8/9* and *Mmp9* genes (Fig. 3d). Importantly, whereas pretreatment of mice with B16F10 TDFs (Fig. 3e) increased the efficacy of lung colonization by intravenously injected B16F10 cells, this effect was completely reversed by addition of ralimetinib (Fig. 3f,g).

Subsequent genetic studies revealed that inducible whole-body ablation of p38α/*Mapk14* (*Mapk14*$^{\Delta/\Delta}$, achieved by tamoxifen treatment of *Ubc9-CreER Mapk14*$^{fl/fl}$ mice; Extended Data Fig. 3b) notably attenuated TDF-elicited events in the lungs, including downregulation of IFNAR1 (Extended Data Fig. 3c), myeloid infiltration (Fig. 3h) and fibronectin accumulation (Fig. 3i). Importantly, these effects of *Mapk14* ablation were reversed by additional deletion of *Ifnar1* (Fig. 3h,i), indicating a pivotal role of p38 kinase and the downstream consequences of its activation (such as IFNAR1 downregulation) in the TDF-stimulated generation of a pre-metastatic niche.

As a complementary approach, we used another mouse model (*Ifnar1*^{S526A} knock-in mice, termed 'SA'), where this mutation within the IFNAR1 phospho-degron renders IFNAR1 insensitive to p38-driven phosphorylation, ubiquitination and degradation[23,24].

Fig. 3 | p38α is essential for generation of the pre-metastatic niche. a, A representative immunofluorescence staining of IFNAR1 (left) and quantification of IFNAR1 level (right) in the lung tissues from WT mice treated with SFM, B16F10 TCM plus vehicle or p38 inhibitor ralimetinib (LY2228820). Scale bar, 100 μm. Quantitative data are shown as mean ± s.e.m. ($n = 4$ mice per group). Two-tailed unpaired *t*-test was performed for the comparisons between two groups. **b**, A representative immunofluorescence staining of CD11b (left) and quantification of CD11b$^+$ cells (right) in the lung tissues from WT mice treated with B16F10 TCM plus vehicle or p38 inhibitor LY2228820. Scale bar, 100 μm. Quantitative data are shown as mean ± s.e.m. ($n = 5$ mice per group). Two-tailed unpaired *t*-test was performed for the comparison. **c**, A representative immunofluorescence staining of fibronectin (left) and quantification of fibronectin level (right) in the lung tissues from WT mice treated with B16F10 TCM plus vehicle or p38 inhibitor LY2228820. Scale bar, 100 μm. Quantitative data are shown as mean ± s.e.m. ($n = 4$ mice per group). Two-tailed unpaired *t*-test was performed for the comparison. **d**, qPCR analysis of mRNA levels of the niche genes in the lung tissues from WT mice treated with SFM (control, $n = 4$ mice), B16F10 TCM plus vehicle ($n = 6$ mice) or LY2228820 ($n = 3$ mice). Data are shown as mean ± s.e.m. Two-way ANOVA and Tukey's multiple comparisons test were performed. **e**, Schematic illustration for analysis of the tumor cell colonization in the lung of the mice pretreated with SFM (control), B16F10 TCM plus vehicle or LY2228820 followed by intravenous injection of 2×10^5 B16F10 tumor cells per mouse. **f**, Representative lung images and the corresponding H&E-stained lung sections from the mice pretreated with SFM (control), B16F10 TCM plus vehicle or LY2228820 followed by intravenous injection of 2×10^5 B16F10 tumor cells as described in **e**. Scale bar, 1 mm. The experiment was repeated three times independently with similar results. **g**, Quantification of the number of metastatic lesions and total area in the lung tissue sections of the mice as shown in **f**. Data are shown as mean ± s.e.m. ($n = 5$ mice per group). Two-tailed unpaired *t*-test was performed for the comparisons between two groups. **h**, A representative immunofluorescence staining of CD11b (left) and quantification of CD11b$^+$ cells (right) in the lung tissues from tamoxifen-treated *Ubc9-CreER*$^-$ *Mapk14*$^{fl/fl}$ *Ifnar1*$^{+/+}$ (*Mapk14*$^{fl/fl}$ *Ifnar1*$^{+/+}$), *Ubc9-CreER*$^+$ *Mapk14*$^{fl/fl}$ *Ifnar1*$^{+/+}$ (*Mapk14*$^{\Delta/\Delta}$*Ifnar1*$^{+/+}$), *Ubc9-CreER*$^-$ *Mapk14*$^{fl/fl}$ *Ifnar1*$^{-/-}$ (*Mapk14*$^{fl/fl}$*Ifnar1*$^{-/-}$) and *Ubc9-CreER*$^+$ *Mapk14*$^{fl/fl}$ *Ifnar1*$^{-/-}$ (*Mapk14*$^{\Delta/\Delta}$*Ifnar1*$^{-/-}$) mice treated with SFM or B16F10 TCM (100 μl i.v., 3x per week for 3 weeks). Scale bar, 100 μm. Quantitative data are shown as mean ± s.e.m. ($n = 5$ mice per group). Two-way ANOVA and Tukey's multiple comparisons test were performed. **i**, A representative immunofluorescence staining of fibronectin (left) and the quantification of fibronectin level (right) in the lung tissues from tamoxifen-treated *Ubc9-CreER*$^-$ *Mapk14*$^{fl/fl}$ *Ifnar1*$^{+/+}$ (*Mapk14*$^{fl/fl}$ *Ifnar1*$^{+/+}$), *Ubc9-CreER*$^+$ *Mapk14*$^{fl/fl}$ *Ifnar1*$^{+/+}$ (*Mapk14*$^{\Delta/\Delta}$*Ifnar1*$^{+/+}$), *Ubc9-CreER*$^-$ *Mapk14*$^{fl/fl}$ *Ifnar1*$^{-/-}$ (*Mapk14*$^{fl/fl}$*Ifnar1*$^{-/-}$) and *Ubc9-CreER*$^+$ *Mapk14*$^{fl/fl}$ *Ifnar1*$^{-/-}$ (*Mapk14*$^{\Delta/\Delta}$*Ifnar1*$^{-/-}$) mice treated with SFM or B16F10 TCM (100 μl i.v., 3x per week for 3 weeks). Scale bar, 100 μm. Quantitative data are shown as mean ± s.e.m. ($n = 4$ mice in all SFM-treated groups, $n = 8$ mice in TCM-treated *Mapk14*$^{fl/fl}$*Ifnar1*$^{+/+}$ and *Mapk14*$^{\Delta/\Delta}$*Ifnar1*$^{+/+}$ groups, $n = 4$ mice in TCM-treated *Mapk14*$^{fl/fl}$*Ifnar1*$^{-/-}$ and *Mapk14*$^{\Delta/\Delta}$*Ifnar1*$^{-/-}$ groups). Two-way ANOVA and Tukey's multiple comparisons test were performed. TCM-LY, combination of TCM with LY2228820.

These SA mice also suppress distant metastases in the genetically engineered and transplanted melanoma models[17,18]. Upon administration of B16F10 TDFs, lungs of these mice retained IFNAR1 (Extended Data Fig. 4a) and sustained the expression of the IFN-stimulated genes (assessed by RNA sequencing; Fig. 4a), including *Stat1*, *Irf7* and *Ifitm3* (otherwise decreased by TDFs;

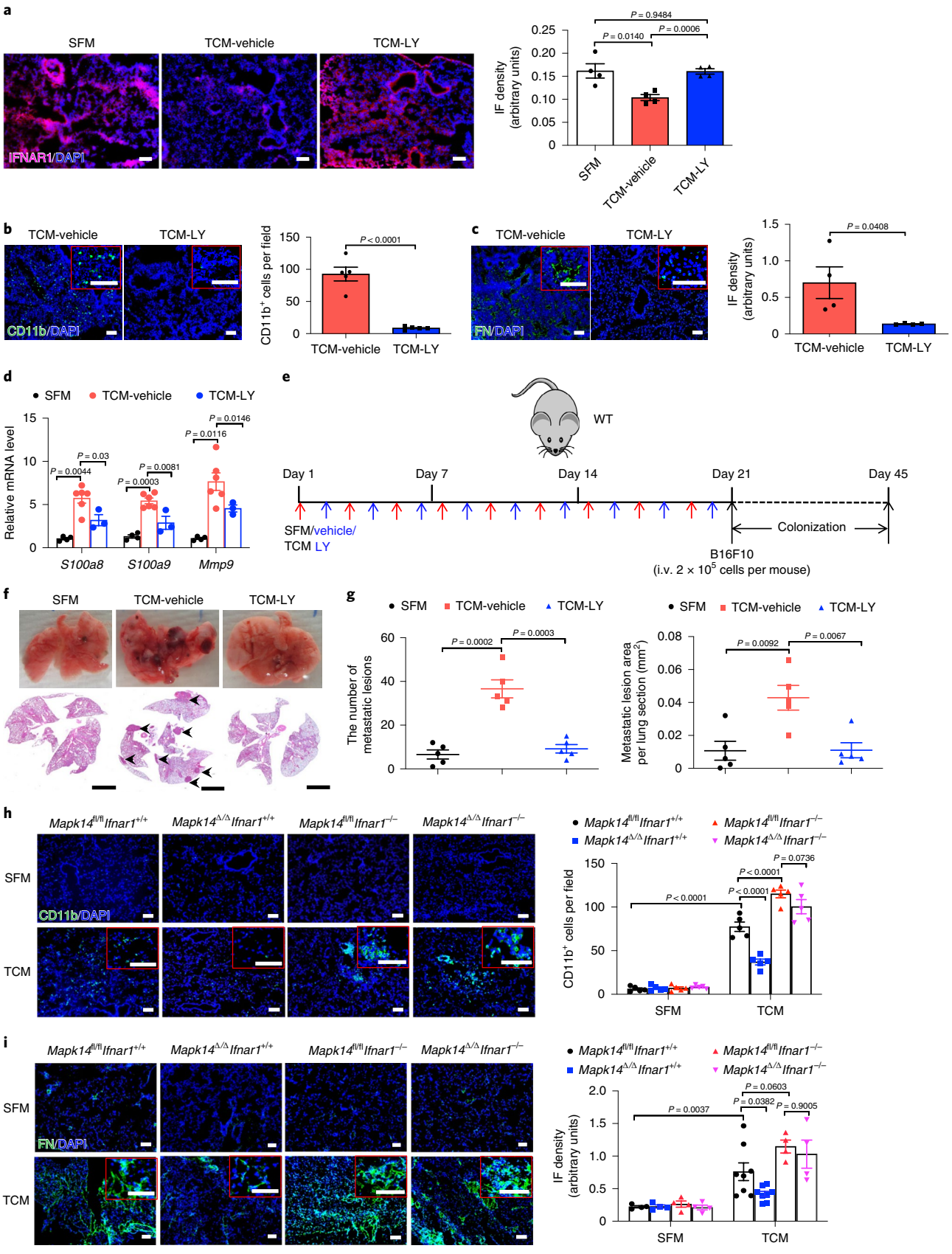

Extended Data Fig. 4b). Importantly, TDF treatment elicited a less pronounced pre-metastatic niche as in the lungs from SA (compared with WT) mice, manifested by differences in expression of *S100a8/9* and *Mmp9* (Fig. 4b), myeloid infiltration (Fig. 4c) and fibronectin deposition (Fig. 4d). Furthermore, B16F10 TDFs did not promote metastatic disease and related death in SA mice bearing subcutaneous B16F1 tumors (Extended Data Fig. 4c–g).

In addition, pretreatment of animals with B16F10 TDFs (Fig. 4e) followed by administration of B16F10-TdTomato cells increased lung colonization in WT but not SA mice (Fig. 4f–h and Extended Data Fig. 4h). Importantly, TDF-pretreated SA mice displayed a notably lesser colonization compared with WT animals. A similar decrease in lung colonization was also observed in TDF-pretreated *Mapk14*$^{\Delta/\Delta}$ mice (Fig. 4f–h), further indicating that TDF-induced p38 activation and its downstream consequences (such as downregulation of IFNAR1) are important for the generation of a pre-metastatic niche.

p38α-mediated induction of the neutrophil-attracting chemokines stimulates malignant cell colonization in the lungs. Characterization of leukocytes in the lungs of WT mice treated with TDFs revealed a predominance of polymorphonuclear myeloid cells (Extended Data Fig. 5a). Numbers of these cells were decreased in the lungs of SA mice (Extended Data Fig. 5a) or WT mice treated with p38 inhibitor (Fig. 5a). These cells exhibited neutrophil markers (CD45$^+$CD11b$^+$Ly6G$^+$Ly6C^{low}) and undetectable immune suppressive properties ex vivo (Extended Data Fig. 5b,c), suggesting that these cells are not myeloid-derived suppressors[25,26]. Together with results reported in melanoma tumor-bearing *Ifnar1*$^{-/-}$ mice[27], these data are consistent with neutrophils being the major type of myeloid cells that infiltrate the lungs downstream of TDF-induced activation of p38 kinase.

Indeed, careful examination and validation of gene expression profiles revealed increased levels of several chemokines known to attract neutrophils (including *Cxcl1*, *Cxcl3* and *Cxcl5*) in the lungs of B16F10 TDF-treated WT mice (Fig. 5b). TDFs from pancreatic and mammary adenocarcinoma cells also increased expression of these genes in vitro (Extended Data Fig. 5d). Induction of chemokine expression in vivo was notably less pronounced in either SA mice (Fig. 5a,c) or WT mice treated with B16F1 TDFs (Extended Data Fig. 5e) or WT that received B16F10 TDFs along with ralimetinib (Fig. 5d). These results suggest that TDF-induced p38 activation and IFNAR1 downregulation trigger elevated expression of the neutrophil-attracting chemokines. Indeed, treatment of mice with an inhibitor of CXCR2 (a receptor for CXCL1, CXCL3 and CXCL5) decreased the numbers of lung neutrophils (Extended Data Fig. 5f), suggesting an important role of the CXCR2 ligands in TDF-induced myeloid pulmonary infiltration.

We next sought to define the mechanistic relationship among p38-driven downregulation of IFNAR1, increased expression of CXCR2-activating chemokines, pulmonary neutrophil infiltration and metastatic colonization. Adenoviral delivery of *Cxcl1* to the lungs of SA mice (Fig. 5e) increased *Cxcl1* expression (Extended Data Fig. 5g) and lung infiltration with myeloid cells (Extended Data Fig. 5h), including neutrophils (Fig. 5f). Remarkably, whereas lungs from SA mice intravenously inoculated with B16F10-TdTomato cells displayed few melanoma cells and virtually no macro-metastatic lesions (Fig. 4f,g), expression of *Cxcl1* in the lungs of SA mice robustly reversed this phenotype and sufficed to enable the metastatic colonization in these animals (Fig. 5g–i). Collectively, these data suggest that p38-driven inactivation of IFNAR1 leads to an induction in expression of CXCL1 (and likely of similarly acting chemokines) to recruit neutrophils and, in the presence of malignant cells, to stimulate the metastatic colonization.

The intratumoral fibroblasts are the major source of CXCL1 that recruits the CD45$^+$CD11b$^+$Ly6G$^+$Ly6C^{low} cells to the primary tumor microenvironment[28]. We found that primary WT lung fibroblasts responded to TDF treatment in vitro with a robust induction of *Cxcl1/3/5* expression; this induction was even greater in *Ifnar1*$^{-/-}$ cells (Fig. 6a). A notably less pronounced chemokine expression was observed in lung fibroblasts isolated from SA or *Mapk14*$^{\Delta/\Delta}$ mice but not in mice lacking both p38 and IFNAR1 (Fig. 6a). Importantly, p38 activation was not affected by the IFNAR1 status (Extended Data Fig. 6a,b). Collectively, these data suggest that p38-driven downregulation of IFNAR1 provides a license for lung fibroblasts to increase the expression of the neutrophil-recruiting chemokines.

We next examined putative mechanisms underlying the regulation of chemokine expression in TDF-treated WT and SA lung fibroblasts. No notable differences in the *Cxcl1* messenger RNA half-life were detected under these conditions (Extended Data Fig. 6c). In pancreatic cancer cells harboring activated Myc, transcriptional activation of the *Cxcl1* promoter depends on trimethylation of Lys4 residue of histone H3 (ref. [29]); however, we did not find differences in this H3K4me3 modification between TDF-treated WT and SA lung fibroblasts (Extended Data Fig. 6d). Instead, we found that expression of the lysine methyltransferase *Setdb2* (known to be induced by type I IFN and to regulate the *Cxcl1* promoter[30,31]) was suppressed by TDFs in WT but not SA fibroblasts (Extended Data Fig. 6e,f). Accordingly, TDF treatment of WT (but not SA)

Fig. 4 | p38α-driven inactivation of the type I IFN pathway drives the formation of a pre-metastatic niche in the lungs. a, The heatmap and gene set enrichment analysis of type I IFN signature genes in the lung tissues of WT and SA mice treated with B16F10 TCM (100 µl i.v., 3x per week for 3 weeks). Expression values are represented as colors, where the range of colors (red, pink, light blue, dark blue) shows the range of expression values (high, moderate, low, lowest). $n=2$ mice per group. NES, normalized enrichment score; FDR, false discovery rate. **b**, qPCR analysis of mRNA levels of indicated genes in the lung tissues from WT and SA mice treated with SFM or B16F10 TCM (100 µl i.v., 3x per week for 3 weeks). Data are shown as mean ± s.e.m. ($n=3$ mice per group). Two-way ANOVA and Tukey's multiple comparisons test were performed. **c**, A representative immunofluorescence staining of CD11b$^+$ (left) and quantification of CD11b$^+$ cells (right) in the lung tissues from WT and SA mice treated with SFM or B16F10 TCM (100 µl i.v., 3x per week for 3 weeks). Scale bar, 100 µm. Quantitative data are shown as mean ± s.e.m. ($n=4$ mice per group). Two-way ANOVA and Sidak's multiple comparisons test were performed. **d**, A representative immunofluorescence staining of fibronectin (left) and quantification of fibronectin level (right) in the lung tissues from WT and SA mice treated with SFM or B16F10 TCM (100 µl i.v., 3x per week for 3 weeks). Scale bar, 100 µm. Quantitative data are shown as mean ± s.e.m. ($n=5$ mice per group). Two-way ANOVA and Sidak's multiple comparisons test were performed. **e**, Schematic illustration for analysis of the tumor cell colonization in the lung of WT, SA and tamoxifen-treated *Mapk14*$^{fl/fl}$*Ubc9CreER*$^-$ (*Mapk14*$^{fl/fl}$) and *Mapk14*$^{fl/fl}$*Ubc9CreER*$^+$ (*Mapk14*$^{\Delta/\Delta}$, p38α knockout in the whole body) mice pretreated with SFM or B16F10 TCM (100 µl i.v., 3x per week for 3 weeks) followed by intravenous injection of 5×10^5 B16F10-TdTomato cells. **f**, Representative lung images and the corresponding H&E-stained lung sections of the indicated mice as described in **e**. Scale bar, 1 mm. Similar results were obtained from three independent experiments. **g**, The percentage of TdTomato$^+$ tumor cells analyzed by flow cytometry in the lung tissues of indicated mice as described in **e**. Data are shown as mean ± s.e.m. ($n=3$ mice for SFM-treated WT and SA groups, $n=3$ mice for TCM-treated *Mapk14*$^{fl/fl}$ and *Mapk14*$^{\Delta/\Delta}$ groups, $n=4$ mice for TCM-treated WT group, $n=5$ for TCM-treated SA group). Two-tailed unpaired *t*-test was performed for the comparisons between two groups. **h**, Quantification of metastatic lesion area in the lung tissues of indicated mice as described in **e**. Data are shown as mean ± s.e.m. ($n=4$ mice for SFM-treated WT and SA groups and TCM-treated WT group, $n=3$ mice for TCM-treated *Mapk14*$^{fl/fl}$ and *Mapk14*$^{\Delta/\Delta}$ groups, $n=5$ mice for TCM-treated SA group). Two-tailed unpaired *t*-test was performed for the comparisons between groups.

lung fibroblasts elicited a decreased trimethylation of histone H3 Lys9 (H3K9me3) on the *Cxcl1* promoter (Fig. 6b); this result is consistent with transcriptional de-repression of this gene as a putative mechanism of *Cxcl1* induction.

TDF-induced p38α-dependent expression of FAP in the lungs plays a key role in the generation of a pre-metastatic niche. Remodeling of the extracellular matrix in a pre-metastatic niche requires activation of lung fibroblasts[2,4,10,32]. Intra-tumoral fibroblasts exposed to TDFs are

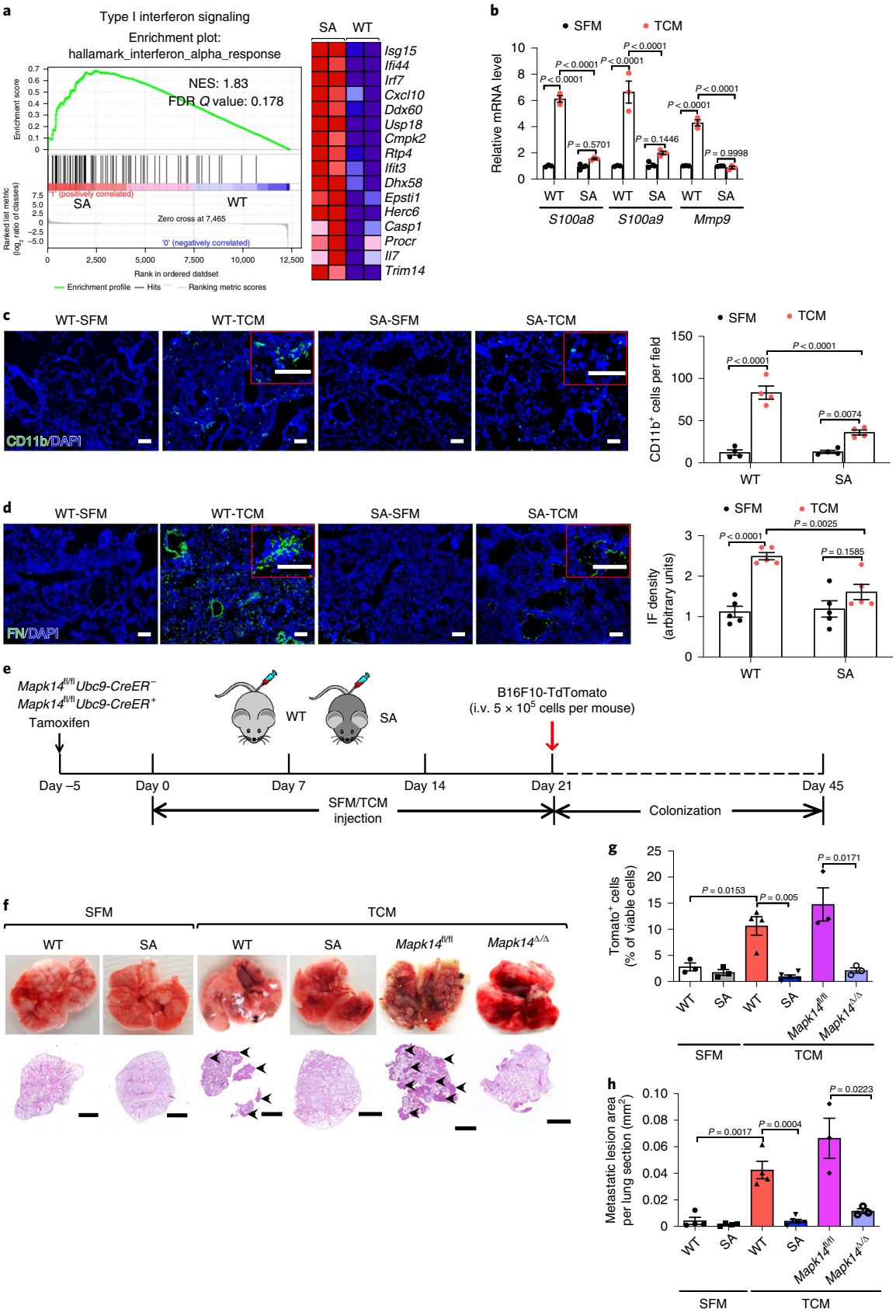

known to become activated and express several markers of this activation including the FAP protease[19–21], which in normal adult tissues is predominantly expressed in bone marrow[33]. Intriguingly, treatment of WT mice with TDFs led to expression of FAP in the lungs (Fig. 6c). Furthermore, TDFs upregulated FAP cell surface levels on WT (but not SA) lung fibroblasts in vitro (Extended Data Fig. 6g), indicating the role of IFNAR1 in suppressing FAP levels.

Accordingly, TDF-induced expression of FAP in the lungs was notably less pronounced in SA mice (Fig. 6c), or in WT mice treated with ralimetinib (Extended Data Fig. 6h) or upon ablation of *Mapk14* (Fig. 6d). In the last case, the phenotype was promptly reversed by genetic deletion of *Ifnar1* (Fig. 6d). Remarkably, genetic ablation of *Fap* in mice[34] notably interfered with the TDF-induced fibronectin accumulation (Fig. 6e) as well as with expression of *Cxcl1*, *Cxcl3* and *Cxcl5* (Fig. 6f); and neutrophil infiltration (Fig. 6g) in vivo. Likewise, despite exhibiting a comparable extent of p38 activation (Extended Data Fig. 6i) and of IFNAR1 downregulation (Extended Data Fig. 6j), TDF-treated lung fibroblasts, which either completely lacked FAP or harbored catalytically inactive FAP^{S624A} mutant (that expressed comparable to WT levels of FAP; Extended Data Fig. 6k,l), exhibited lower levels of *Cxcl1/3/5* mRNA (Fig. 6h). Conversely, treatment of FAP-null fibroblasts with a recombinant, soluble and enzymatically active extracellular domain (ECD) of FAP partially increased levels of *Cxcl1/3/5* (Fig. 6h). Collectively, these data suggest that TDF-induced activation of p38 and downstream pathways in lung fibroblasts induce FAP, which plays a key role in the generation of a pre-metastatic niche.

To further test this hypothesis, we ablated p38α in the fibroblasts by treating *Col1a2-CreER Mapk14*$^{fl/fl}$ mice with tamoxifen to produce *Mapk14*$^{\Delta Fib}$ mice (Extended Data Fig. 7a). These (and appropriate control) animals were administered with TDFs derived from metastatic B16F10 melanoma or from MH6499c4 pancreatic adenocarcinoma. Examination of the lungs of these mice revealed that ablation of p38α in the fibroblasts notably attenuated the TDF-induced events, including downregulation of IFNAR1 (Extended Data Fig. 7b), an increase in the levels of FAP (Fig. 7a) and fibronectin (Fig. 7b), expression of the niche and chemokine genes, and pulmonary neutrophil infiltration either before or after malignant cell inoculation (Fig. 7c,d and Extended Data Fig. 7c–e). Consistent with these data, a decreased colonization of the lungs of TDF-treated *Mapk14*$^{\Delta Fib}$ mice by malignant cells (Fig. 7e–g and Extended Data Fig. 7f) further indicates that p38 status in the fibroblasts is important for the formation of the pre-metastatic niche.

Targeting p38α in the context of (neo)adjuvant therapy suppresses pulmonary melanoma metastases. We mimicked the TDF-induced activation of p38 and downregulation of IFNAR1 by ablating this receptor specifically in fibroblasts (*Ifnar1*$^{\Delta Fib}$, achieved by tamoxifen treatment of *Col1a2-CreER Ifnar1*$^{fl/fl}$ mice; Extended Data Fig. 8a). Increased chemokine expression (Extended Data Fig. 8b), neutrophil infiltration (Extended Data Fig. 8c,d) and lung colonization by intravenously administered B16F10 cells (Fig. 8a,b) were observed in the *Ifnar1*$^{\Delta Fib}$ mice compared with control animals. We then assessed the importance of the p38 activation in the fibroblasts in a spontaneous metastatic process using a model wherein B16F10 tumor-bearing mice underwent survival surgery to remove primary tumors (Extended Data Fig. 8e) and then were analyzed for lung metastases and animal survival. Under these conditions, *Mapk14* ablation notably decreased the number of lung lesions (Fig. 8c,d) and prolonged animal survival (Fig. 8e), further supporting an important role of p38α in fibroblasts in development of metastatic disease.

This genetic evidence prompted us to examine whether pharmacologic p38 inhibitors such as ralimetinib and SB203580 were suitable for the adjuvant therapy of melanoma (Fig. 8f). TDFs from ralimetinib-treated B16F10 cells induced a modestly lesser activation of p38 and downregulation of IFNAR1 in vitro (Extended Data Fig. 8f,g). In vivo administration of p38 inhibitors elicited a modest effect on primary tumor growth; thus, we modified the timing of the surgical resection of primary tumors to remove tumors of similar volume in all groups (Extended Data Fig. 8h), followed by additional treatments with vehicle or ralimetinib or SB203580. Under these conditions, p38 inhibitors elicited a suppressive effect on lung metastases (Fig. 8g,h) and notably prolonged animal survival (Fig. 8i).

Discussion

Work presented here supports a model (Fig. 8j) where the pro-metastatic secretome-driven activation of p38α kinase in lung fibroblasts represents a pivotal step in forming a pre-metastatic niche, manifested by accumulation of fibronectin and entrapment of neutrophils. Both of these events require TDF-stimulated expression of FAP, which also contributes to induction of the CXCR2-interacting chemokines that recruit neutrophils. Given that p38 supports growth of primary tumors[35], including lung cancers[36], TDF-driven p38 activation in lung fibroblasts may generate a similar protective environment for survival and growth of cancer cells within both primary and secondary metastatic lung tumors. Indeed, p38α plays an important role in metastatic colonization (Fig. 8c–e and see ref. [37]).

Fig. 5 | p38α activation-mediated induction of the neutrophil-attracting chemokines stimulates melanoma cell colonization in the lungs. a, Representative flow cytometry analysis of myeloid cell subpopulations (total myeloid cells, $CD45^+CD11b^+$; granulocytes, $CD45^+CD11b^+Ly\text{-}6G^+Ly\text{-}6C^{low}$; monocytes, $CD45^+CD11b^+Ly\text{-}6G^-Ly\text{-}6C^+$) (above) and quantification of these cell subpopulations (below) in the lung tissues of WT mice treated with B16F10 TCM plus vehicle or p38 inhibitor LY2228820. Quantitative data are shown as mean ± s.e.m. ($n = 4$ mice per group). Two-tailed unpaired *t*-test was performed for the comparison. **b**, Heatmap of gene expression of chemokines in the lung tissues of WT and SA mice treated with B16F10 TCM (100 µl i.v., 3x per week for 3 weeks). Expression values are represented as colors, where the range of colors (red, pink, light blue, dark blue) shows the range of expression values (high, moderate, low, lowest). The red asterisks denote core enriched genes in WT mice compared with SA mice. **c**, qPCR analysis of mRNA levels of the indicated chemokines in the lung tissues of WT and SA mice treated with SFM or B16F10 TCM (100 µl i.v., 3x per week for 3 weeks). Data are shown as mean ± s.e.m. ($n = 3$ mice for SFM group, $n = 4$ mice for TCM group). Two-way ANOVA and Tukey's multiple comparisons test were performed. **d**, qPCR analysis of mRNA levels of the indicated chemokines in the lung tissues of WT mice treated with SFM ($n = 3$ mice), B16F10 TCM plus vehicle ($n = 6$ mice) or p38 inhibitor LY2228820 ($n = 4$ mice). Data are shown as mean ± s.e.m. Two-way ANOVA and Tukey's multiple comparisons test were performed. **e**, Schematic illustration for analysis of the tumor cell colonization in the lungs of SA mice engineered to re-express CXCL1 by intranasally delivered adenoviruses. **f**, Representative flow cytometry analysis of neutrophils (above) and quantification of the percentage of neutrophils (below) in the lung tissues of SA mice as described in **e**. Quantitative data are shown as mean ± s.e.m. ($n = 4$ mice for Ad-ctrl group, $n = 5$ for AdCXCL1 group). Two-tailed unpaired *t*-test was performed for the comparison. **g**, Representative flow cytometry analysis of $TdTomato^+$ tumor cells (above) and the quantification (below) in the lung tissues of SA mice as described in **e**. Quantitative data are shown as mean ± s.e.m. ($n = 4$ mice for Ad-ctrl group, $n = 5$ mice for AdCXCL1 group). Two-tailed unpaired *t*-test was performed for the comparison. **h**, Representative lung images and the corresponding H&E-stained lung sections of SA mice as described in **e**. Scale bar, 1 mm. Similar results were obtained from three independent experiments. **i**, Quantification of metastatic lesion area in the lung tissues of SA mice as shown in **h**. Data are shown as mean ± s.e.m. ($n = 4$ mice per group). Two-tailed unpaired *t*-test was performed for the comparison. FSC-A, forward scatter area.

It is also plausible that epithelial and/or endothelial lung cells (implicated in the niche formation[4,11]) exposed to TDFs produce additional factors (for example, cytokines) that can further activate p38α kinase in lung fibroblasts, thereby amplifying the entire pro-metastatic pathway. In addition to fibroblasts, other FAP- or collagen-expressing cells (for example, macrophages, vascular smooth muscle cells, fibrocytes

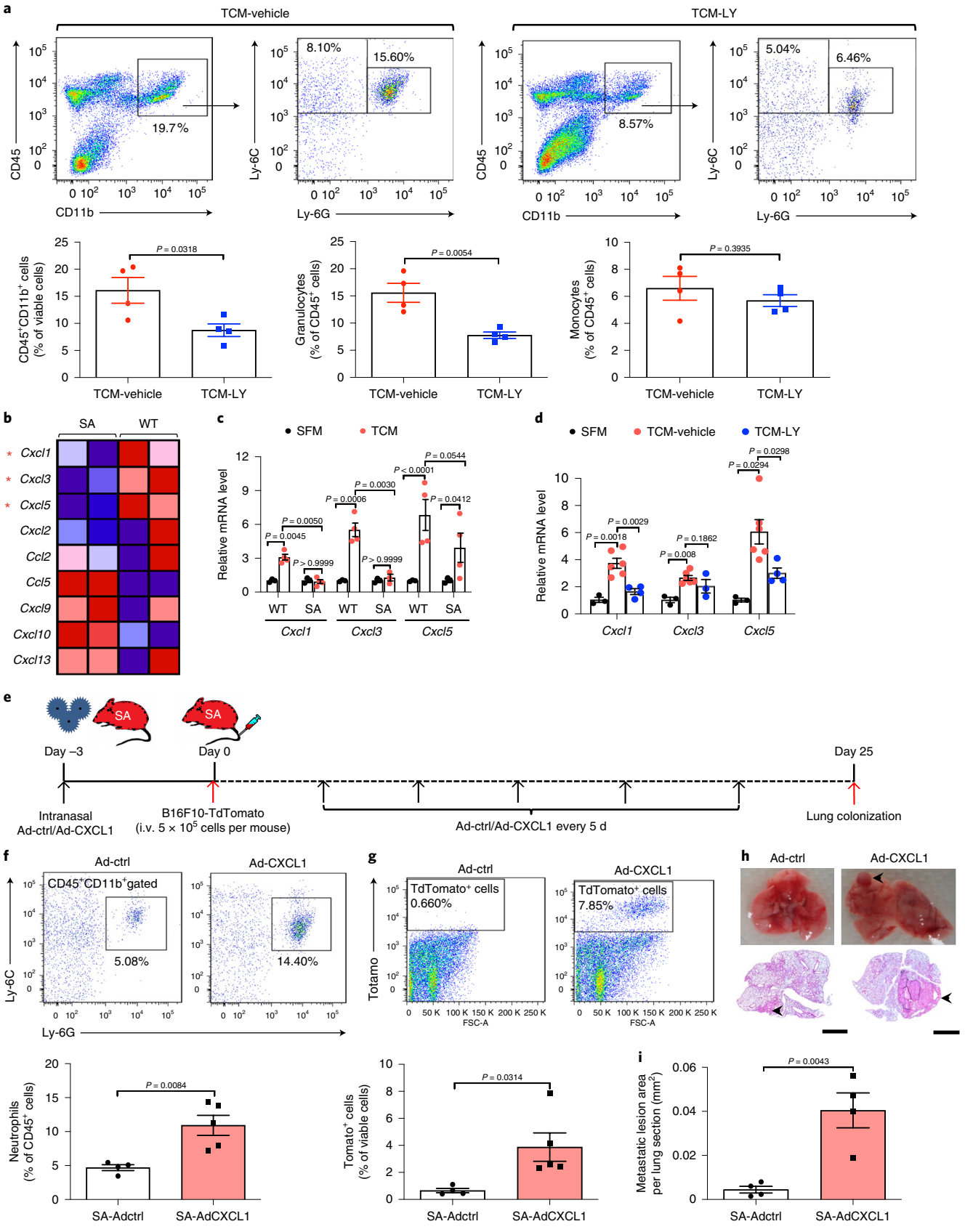

or pericytes) were implicated in the development of a pre-metastatic niche[38–41]; the role of p38α kinase in these cells should not be ruled out.

It is likely that many diverse soluble factors and extracellular vesicles within the malignant cell secretome (thoroughly cataloged in refs. [3,11]) are responsible for activation p38α kinase and for triggering the generation of the pre-metastatic niche. For example, pro-inflammatory cytokines[16], vascular endothelial growth factor[42] and the ligands for the pathogen recognition receptors[43] (such as lipids/protein/nucleic acids and other biomolecules present in the extracellular vesicles[44–46]) were all associated with p38 activation and IFNAR1 downregulation. In this context, p38 kinase acts as an integrator of inputs from malignant cells and as a key translator of these signals into downstream events leading to the formation of a pulmonary pre-metastatic niche.

Whereas genetic studies reported here emphasize the essential role of p38α/*MAPK14*, the importance of other p38 isoforms in the metastatic process cannot be ruled out. Phosphorylation mediated by p38α is pivotal for TDF-driven proteolytic loss of IFNAR1 (refs. [16,18]). Consistently, current data supporting the importance of IFNAR1 inactivation in the generation of the pre-metastatic niche and stimulation of metastases are consistent with studies in melanoma and breast cancer models demonstrating that IFNAR1-null mice exhibited a greater metastatic disease[27,47] and that animals resistant to IFNAR1 downregulation (SA mice) were deficient in distant metastases[17,18].

TDFs induce FAP in the lungs, which otherwise express little (if any) of this protease (see refs. [33,48] and Fig. 6). FAP has been well characterized as a marker of activated reactive/inflammatory fibroblasts including cancer-associated fibroblasts[19,21,49,50]. Although FAP is found in the tumor microenvironment of many human and mouse primary tumors[19,21], primary subcutaneously growing B16F10 tumors exhibited negligible levels of FAP (data not shown). It appears that fibroblasts (and possibly other cells) in the lungs display a distinct ability to respond to TDFs with an induction of FAP. Understanding of the molecular basis of these distinctive characteristics as well as how inactivation of IFNAR1 leads to FAP expression is of major interest and warrants further investigations.

FAP mediates production of fibronectin (Fig. 6); the latter, along with other elements of reshaped extracellular matrix, helps to entrap the recruited neutrophils in the lungs[4,10,11]. Delineation of the mechanisms underlying the effects of FAP on expression of the neutrophil-attracting chemokines requires further investigation. Given that knock-in of inactive FAP^{S624A} impeded the induction of *Cxcl1/3/5*, whereas treatment of FAP-null lung fibroblasts with an active recombinant FAP partially restored chemokine expression (Fig. 6h), it is plausible that protease activity of FAP toward polypeptide substrates of cell surface or/and extracellular matrix acts to produce factors stimulating expression of these chemokines. However, a noncatalytic role of FAP in neutrophil recruitment (similar to a recently reported role of dipeptidase-1 (ref. [51])) should not be ruled out. Regardless of these considerations, current data clearly suggest an important mechanistic role of FAP in the formation of a pre-metastatic niche. This function is consistent with suppressed metastases of pancreatic ductal adenocarcinoma in *Fap*-null mice[52].

Neutrophils represented the bulk of myeloid cells in the lungs from animals treated with TDFs. Elegant recent studies demonstrated that neutrophils attracted to inflamed lungs harboring already disseminated yet dormant malignant cells play a critically important role in re-awakening these cells and in stimulation of lung colonization[53]. Future studies will be required to decipher the commonalities and dissimilarities between the mechanisms underlying stimulation of metastatic colonization in the context of either generation of a pre-metastatic niche or disruption of the dormant niche in the lungs.

Although metastases are the major cause of cancer-related patient deaths, the pace of development of therapeutic modalities targeting metastatic disease is slower than the progress achieved in the efforts to control growth of primary tumors[54]. It was reported that p38 inhibitors such as SB203580 administered in immune-compromised settings can activate dormant cancer cells and actually stimulate lung metastatic colonization[55]. Yet, in the model of metastatic pulmonary colonization in immune-competent mice, SB203580 decreased metastatic load[56]. Importantly, given the efficacy of p38 inhibitors (such as SB203580 or ralimetinib) shown in this work, these agents might be of translational importance in the context of adjuvant or/and neoadjuvant therapy.

Furthermore, inhibition of p38 kinase may improve the anti-tumorigenic effect of the cytotoxic lymphocytes that can kill these cancer cells[57], thereby contributing to the robust anti-metastatic effects of p38 inhibitors observed in this study in an immune-competent model. Whereas ralimetinib exhibited an acceptable safety profile and modest activity in a phase I trial for aromatase refractory metastatic breast cancer[58], future clinical studies

Fig. 6 | TDF-induced p38α-dependent expression of FAP in the lungs plays a key role in the generation of the pre-metastatic niche. a, qPCR analysis of indicated chemokine mRNA levels in the lung fibroblasts (from indicated mice) at 6 h after SFM or B16F10 TCM treatment in vitro. Data are shown as mean ± s.e.m. ($n = 5$ biologically independent samples). Two-way ANOVA and Tukey's multiple comparisons test were performed. **b**, ChIP analysis of H3K9me3 binding to the *Cxcl1* promoter in the isolated WT and SA lung fibroblasts treated with SFM or B16F10 TCM for 12 h. Data are shown as mean ± s.e.m. ($n = 4$ independent experiments). Two-way ANOVA and Sidak's multiple comparisons test were performed. **c**, A representative immunofluorescence staining of FAP (left) and quantification of FAP^+ cells (right) in the lung tissues of WT and SA mice treated with SFM or B16F10 TCM (100 µl i.v., 3x per week for 3 weeks). Scale bar, 100 µm. Quantitative data are shown as mean ± s.e.m. ($n = 5$ mice per group). Two-way ANOVA and Sidak's multiple comparisons test were performed. **d**, A representative immunofluorescence staining of FAP (left) and quantification of FAP^+ cells (right) in the lung tissues of indicated mice treated with SFM or B16F10 TCM (100 µl i.v., 3x per week for 3 weeks). Scale bar, 100 µm. Quantitative data are shown as mean ± s.e.m. ($n = 4$ mice per group). Two-way ANOVA and Tukey's multiple comparisons test were performed. **e**, A representative immunofluorescence staining of fibronectin (left) and quantification of fibronectin level (right) in the lung tissues from WT and $Fap^{-/-}$ mice treated with SFM or B16F10 TCM (100 µl i.v., 3x per week for 3 weeks). Scale bar, 100 µm. Quantitative data are shown as mean ± s.e.m. ($n = 5$ mice per group). Two-way ANOVA and Sidak's multiple comparisons test were performed. **f**, qPCR analysis of mRNA levels of the indicated chemokines in the lung tissues of WT and $Fap^{-/-}$ mice treated with SFM or B16F10 TCM (100 µl i.v., 3x per week for 3 weeks). Data are shown as mean ± s.e.m. ($n = 3$ mice per group). Two-way ANOVA and Sidak's multiple comparisons test were performed. **g**, Representative flow cytometry analysis of neutrophils (left) and quantification of their percentage (right) in the lung tissues of WT and $Fap^{-/-}$ mice treated with SFM or B16F10 TCM (100 µl i.v., 3x per week for 3 weeks). Quantitative data are shown as mean ± s.e.m. ($n = 3$ mice per group). Two-way ANOVA and Sidak's multiple comparisons test were performed. **h**, qPCR analysis of mRNA levels of the indicated chemokines in the lung fibroblasts isolated from WT, Fap^{S624A} knock-in and $Fap^{-/-}$ mice 6 h after SFM or B16F10 TCM treatment with or without adding FAP ECD (FAP^{ECD}, 0.3 µg ml^{-1}). Data are shown as mean ± s.e.m. $n = 6$ biologically independent samples in SFM- and TCM-treated WT cells and SFM-treated $Fap^{-/-}$ cells, $n = 5$ biologically independent samples in TCM-treated $Fap^{-/-}$ cells, n = 4 biologically independent samples in SFM-treated Fap^{S624A} cells, $n = 3$ biologically independent samples in TCM-treated Fap^{S624A} cells and $Fap^{-/-}$ cells with FAP ECD added. Two-way ANOVA and Tukey's multiple comparisons test were performed.

are required for determining the potential of this agent (as well as other inhibitors of p38 kinases) for adjuvant treatment of metastatic melanoma and, possibly, other highly metastatic cancers.

Methods

Animal studies. All in vivo experiments carried out on mice of C57Bl/6 background were approved by the Institutional Animal Care and Use Committee of

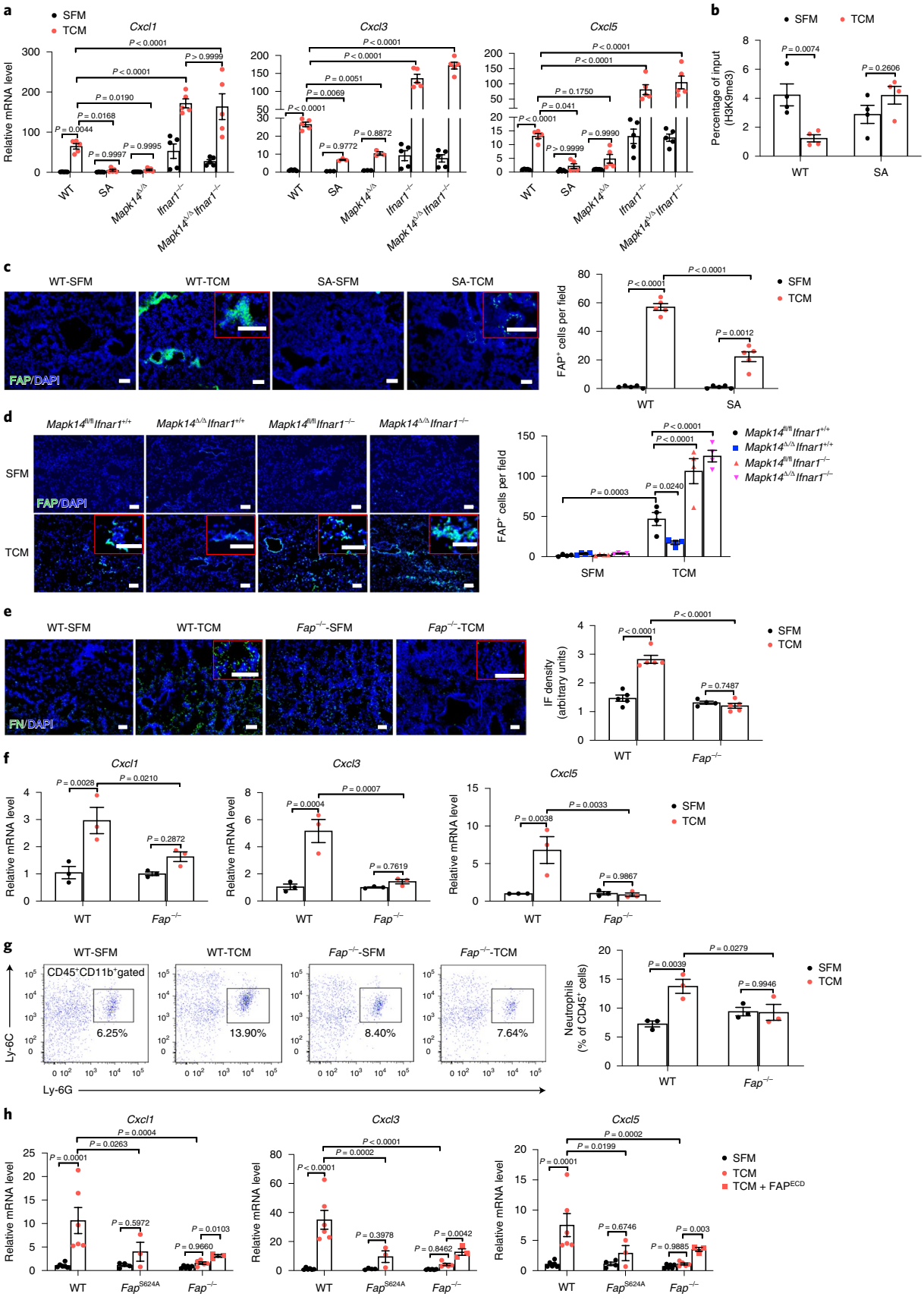

the University of Pennsylvania. Mice were maintained in a specific-pathogen-free facility in accordance with American Association for Laboratory Animal Science guidelines. Littermate *Ifnar1*$^{+/+}$ ('WT') and *Ifnar1*^{S526A} mice (SA)[23] as well as *Fap*$^{-/-}$ mice[34] were described previously. *Ifnar1*$^{-/-}$ mice were generously provided by Dr. Susan Weiss (University of Pennsylvania, Philadelphia, USA). *Ubc9-CreER* mice (gift from E. Brown, University of Pennsylvania) were crossed with *Mapk14*$^{fl/fl}$ mice (generously provided by Yibin Wang, University of California, Los Angeles, USA) and *Ifnar1*$^{-/-}$ mice to generate either *Ubc9-CreER*$^{+/0}$; *Mapk14*$^{fl/fl}$; *Ifnar1*$^{+/+}$ or *Ubc9-CreER*$^{+/0}$; *Mapk14*$^{fl/fl}$; *Ifnar1*$^{-/-}$ littermates. *Col1a2-CreER* mice (obtained from Jackson Laboratory) were crossed with *Mapk14*$^{fl/fl}$ mice or *Ifnar1*$^{fl/fl}$ mice (obtained from Jackson Laboratory) to generate *Col1a2-CreER*$^{+/0}$; *Mapk14*$^{fl/fl}$ *or* *Col1a2-CreER*$^{+/0}$; *Ifnar1*$^{fl/fl}$ littermates, respectively. All of these mice were viable and fertile with no reported abnormalities. The genotyping PCR primers are provided in Supplementary Table 1. Littermate animals from different cages were randomly assigned into experimental groups, which were either co-housed or systematically exposed to other groups' bedding to ensure equal exposure to all groups' microbiota. To induce *Mapk14* deletion in the whole body or specifically in fibroblasts, *Mapk14*$^{fl/fl}$ *Ubc9-CreER*$^{+/0}$ mice *or Mapk14*$^{fl/fl}$ *Col1a2-CreER*$^{+/0}$ mice were given tamoxifen (Sigma, dissolved in maize oil) once daily via oral gavage for 5 consecutive days at a dose of 0.2 mg per gram of body weight per day.

Fap^{S624A} knock-in mice expressing FAP mutant that lacks the protease activity were generated as follows: CRISPR–CAS9 homology directed repair targeting was used to generate a single 1-base pair (bp) change at the S624 site: T to G. WT is 'TCC' which codes for serine and the mutant is 'GCC' which codes for alanine. The CRISPR Guide targets used were Guide no. 2 (sense: 5′-GATGTCTCTACAGTCCT ACGG-3′) for the F8 cell line and Guide no. 5 (sense: 5′-GACAATGTCTCTACAGTCCTA-3′) for the H7 cell line. The single-stranded 158-mer Ultramer homology directed repair template sequence was: sense: 5′-GTA GAC TTT AAA AAC ACA GAG ATG CTT TTG AGC TTG TGT CTG GGG CTG ACC AAT AAC AAT GTC TCT ACA GGC CTA CGG AGG TTA TGT TTC ATC CCT GGC CCT TGC ATC TGG AAC TGG TCT TTT CAA ATG TGG CAT AGC AGT GGC TCC AGT CTC CAG CT -3′. The genotyping PCR primers and sequencing primer are provided in Supplementary Table 1. The genomic DNA amplified a 677-bp fragment of both WT and knock-in mice. Sequencing of this 677-bp PCR product revealed two chromatogram peaks for heterozygous (T/G), one peak each in WT 'T' and homozygous mutant animal 'G'. The S624A knock-in also generated a Stu1 restriction site (AGG|CCT) only in the knock-in mice. Digestion of PCR products with Stu1 yielded 210-bp and 467-bp fragments. The *Fap*^{S624A} knock-in mice were backcrossed with WT C57Bl/6 mice. The homozygotes (mixed background of 129/Sv and C57Bl/6) were used for lung fibroblast isolation.

Lung fibroblast isolation. The lung tissues from 3–5-week-old mice were washed with ice-cold PBS, minced and incubated with 3 ml of solution containing Collagenase II (2 mg ml^{-1}) and DNase I (100 µg ml^{-1}) for 1 h at 37 °C. After stopping digestion by adding equal volumes of fetal bovine serum (FBS), cells were passed through 100-µm and 40-µm filters, spun down, washed and then resuspended with complete medium (DMEM containing 10% FBS and 1% Penicillin-Streptomycin) and cultured overnight. The next day, the nonadherent cells were thoroughly washed off with PBS and the remaining cells were cultured in complete medium for around 1 week before use.

Cell lines and tumor-conditioned medium (TCM) preparation. Mouse melanoma cell lines B16F1 (ATCC CRL-6323) and B16F10 (ATCC CRL-6475) were purchased from ATCC and maintained in DMEM (Gibco) supplemented with 10% FBS (HyClone) and 100 U ml^{-1} Penicillin-Streptomycin (Gibco). Mouse mammary adenocarcinoma cell line E0771 was purchased from CH3 Biosystems (cat. no. 940001) and maintained in RPMI 1640 medium (Gibco) supplemented with 10% FBS and 100 U ml^{-1} Penicillin-Streptomycin according to the instructions. Mouse pancreatic tumor cell clone MH6499c4 was isolated from late-stage primary tumors from a spontaneous tumor model as described before[29]. All of the cell lines were regularly tested for *Mycoplasma*.

Tumor cells were plated on 150-mm cell culture plates and allowed to adhere overnight in growth medium. The next day, when the cells were 80% confluent, growth medium was removed, and the cells were washed with PBS three times and cultured in serum-free medium (SFM) for 48 h. After that, the conditioned medium was collected and filtered with a 0.22-µm filter, and then stored at −80 °C until use. For in vivo treatment, 100 µl of TCM was intravenously injected into mice three times a week for 3 weeks. SFM injection was set as negative control. After that, mice were euthanized and lung tissues were collected for analysis. For in vitro treatment, cells were plated on six-well plates and treated with 1.5 ml of TCM/SFM plus 0.5 ml of complete medium (ratio 3:1) for 6–12 h.

Human samples. Informed consent was obtained from all study participants. Study approval was given by the Institutional Review Board of the University of Pittsburgh. Peripheral blood was aseptically collected into (green top) Na Heparin vacutainer tubes from 40 patients with melanoma (stage I, II, III or IV). The blood was then stored at room temperature (16–30 °C) and processed as follows. The sample was centrifuged for 5 min at 1,000 r.p.m. and without stopping the speed was increased to 1,800–2,000 r.p.m. for 20 min with the brake off. The peripheral blood leukocyte layer between the clear lymphocyte separation medium and upper PBS layer was gently pipetted off. The cells were washed with PBS three times and suspended in medium (Iscov's Modified Dulbecco's Medium, 10% human serum, 1% Penicillin-Streptomycin solution, 1% L-glutamine, 1% MEM nonessential amino acids 10 mM, 1% HEPES buffer solution 1 M) with 10% dimethylsulfoxide for incubation at −80 °C overnight before long-term storage at −140 °C. For recovery, frozen cells were thawed rapidly in a 37 °C water bath. The thawed cells were slowly, but immediately, transferred into 10 ml of PBS and washed with PBS twice before lysis.

Western blot analysis. The human blood leukocytes were lysed with 60 µl of RIPA lysis buffer for 30 min on ice. All of the samples were diluted to the same concentration (3 of 40 samples had too low a concentration and were excluded from the analysis). The immunoblotting analyses were carried out as previously described[16,24]. The following antibodies were purchased and used: phospho-p38 (Thr180/Tyr182) (Cell Signaling Technology, Clone 28B10 cat. no. 9216S, 1:1,000) and p38α (Santa Cruz, Clone C-20 cat. no. sc-535, 1:1,000), GAPDH (Cell Signaling Technology, Clone D16H11 cat. no. 5174S, 1:5,000) and β-Tubulin (Cell Signaling Technology, cat. no. 2146S, 1:5,000). Goat anti-rabbit HRP-conjugated

Fig. 7 | p38α deficiency specifically in fibroblasts impairs the generation of a pre-metastatic niche in the lung. a, A representative immunofluorescence staining of FAP (left) and quantification of FAP level (right) in the lung tissues of tamoxifen-treated *Mapk14*$^{fl/fl}$*Col1a2-CreER*$^{-}$ (*Mapk14*$^{fl/fl}$) and *Mapk14*$^{fl/fl}$ *Col1a2-CreER*$^{+}$ (*Mapk14*$^{\Delta Fib}$, p38α knockout specifically in fibroblasts) mice injected with SFM, B16F10 TCM or MH6499c4 TCM (100 µl i.v., 3x per week for 3 weeks). Scale bar, 100 µm. Quantitative data are shown as mean ± s.e.m. ($n = 6$ mice for SFM- and B16F10 TCM-treated groups, $n = 5$ mice for MH6499c4 TCM-treated group). Two-way ANOVA and Tukey's multiple comparisons test were performed. **b**, A representative immunofluorescence staining of fibronectin (left) and quantification of fibronectin level (right) in the lung tissues of *Mapk14*$^{fl/fl}$ and *Mapk14*$^{\Delta Fib}$ mice injected with SFM, B16F10 TCM or MH6499c4 TCM (100 µl i.v., 3x per week for 3 weeks). Scale bar, 100 µm. Quantitative data are shown as mean ± s.e.m. ($n = 6$ mice for SFM- and B16F10 TCM-treated groups, $n = 5$ mice for MH6499c4 TCM-treated group). Two-way ANOVA and Tukey's multiple comparisons test were performed. **c**, qPCR analysis of mRNA levels of the indicated chemokines and niche genes in the lung tissues of *Mapk14*$^{fl/fl}$ and *Mapk14*$^{\Delta Fib}$ mice injected with SFM, B16F10 TCM or MH6499c4 TCM (100 µl i.v., 3x per week for 3 weeks). Data are shown as mean ± s.e.m. ($n = 6$ mice for SFM-treated group, $n = 5$ mice for B16F10 and MH6499c4 TCM-treated groups). Two-way ANOVA and Tukey's multiple comparisons test were performed. **d**, The percentage (left) and the absolute number of neutrophils (right) analyzed by flow cytometry in the lung tissues of *Mapk14*$^{fl/fl}$ and *Mapk14*$^{\Delta Fib}$ mice injected with SFM, B16F10 TCM or MH6499c4 TCM (100 µl i.v., 3x per week for 3 weeks). Data are shown as mean ± s.e.m. ($n = 6$ mice for SFM- and B16F10 TCM-treated groups, $n = 5$ mice for MH6499c4 TCM-treated group). Two-way ANOVA and Tukey's multiple comparisons test were performed. **e**, The percentage of tumor cells (TdTomato^{+} cells) analyzed by flow cytometry in the lung tissues of *Mapk14*$^{fl/fl}$ and *Mapk14*$^{\Delta Fib}$ mice injected with SFM, B16F10 TCM or MH6499c4 TCM (100 µl i.v., 3x per week for 3 weeks) followed by intravenous injection of 5×10^5 B16F10-TdTomato cells. Data are shown as mean ± s.e.m. ($n = 4$ mice for SFM-treated group, $n = 5$ mice for B16F10 and MH6499c4 TCM-treated groups). Two-way ANOVA and Tukey's multiple comparisons test were performed. **f**, Representative lung images and the corresponding H&E-stained lung sections of *Mapk14*$^{fl/fl}$ and *Mapk14*$^{\Delta Fib}$ mice injected with SFM, B16F10 TCM or MH6499c4 TCM (100 µl i.v., 3x per week for 3 weeks) followed by intravenous injection of 5×10^5 B16F10-TdTomato cells. Scale bar, 1 mm. Similar results were obtained from three independent experiments. **g**, Quantification of metastatic lesion area in the lung sections of indicated mice as shown in **f**. Data are shown as mean ± s.e.m. ($n = 6$ mice for SFM-treated group, $n = 5$ mice for B16F10 and MH6499c4 TCM-treated groups). Two-way ANOVA and Tukey's multiple comparisons test were performed.

IgG (Millipore, cat. no. AP187P, 1:20,000) or Goat anti-mouse HRP-conjugated IgG (Cell Signaling Technology, cat. no. 7076S, 1:20,000) was used as secondary antibody, correspondingly. The intensity of the bands was analyzed by ImageJ and the ratio of phospho-p38 to total p38 was calculated.

Experimental tumor metastasis model. B16F1/B16F10 tumor cells in a single-cell suspension (1×10^5 in 100 µl of PBS) were subcutaneously injected into the right flanks of mice. Tumors were aseptically resected at a volume of ~200 mm^2. After surgery, mice were monitored and killed when moribund. Lung tissues were

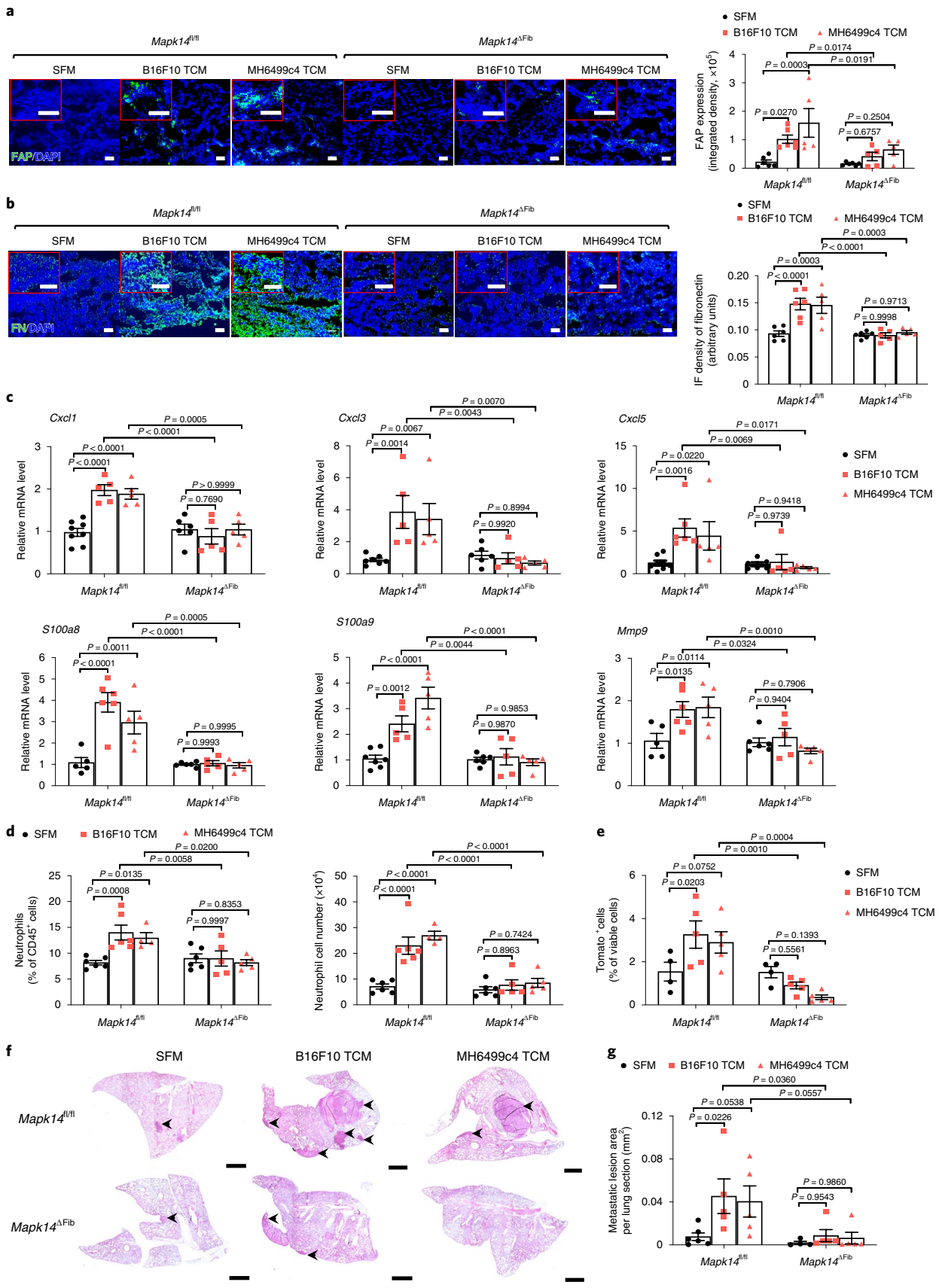

collected, fixed in 4% PFA-PBS (Thermo Fisher Scientific) and hematoxylin and eosin (H&E) stained for lung metastasis analysis.

For tumor cell lung colonization assay, 2×10^5 B16F10 or 5×10^5 B16F10-TdTomato cells per mouse were intravenously injected into mice. Around 3 weeks after tumor cell injection, mice were euthanized and lung tissues were collected and fixed in 4% PFA-PBS for H&E staining.

The composite images of whole H&E-stained lung sections were taken by the Leica DM6000 Widefield microscope. The number and size of tumor metastatic lesions in lung tissues were analyzed by ImageJ.

Adenovirus and chemical inhibitors treatment. Adenovirus-expressing mouse CXCL1 (Ad-CXCL1) and the control adenovirus (Ad-ctrl) were purchased from Applied Biological Materials. Mice were anesthetized with ketamine and xylazine and intranasally delivered with adenoviruses (20 µl per mouse at 2×10^8 plaque-forming units per mouse). After 3 d, these mice were intravenously injected with 5×10^5 B16F10-TdTomato cells and then continually administered with Ad-CXCL1 or Ad-ctrl every 5 d. At day 25 after tumor cell injection, mice were euthanized, and lung tissues were collected for FACS analysis of tumor cells (Tomato$^+$) and fixed in 4% PFA-PBS for H&E staining.

p38 kinase inhibitor LY2228820 (Selleckchem, cat. no. S1494) was dissolved in 1% methylcellulose and administered by oral gavage at the dose of 10 mg kg^{-1} every other day. SB203580 hydrochloride (Tocris Bioscience, cat. no. 1402) was dissolved in sterile water and administered by intraperitoneal injection at the dose of 10 mg kg^{-1} every other day. CXCR2 inhibitor SB225002 (Selleckchem, cat. no. S7651) was dissolved in 2% dimethylsulfoxide + 30% PEG300 + 5% Tween 80 + double-distilled H_2O and administered by oral gavage at the dose of 10 mg kg^{-1}. For adjuvant therapy, 1×10^5 B16F10 tumor cells were subcutaneously injected into WT mice. When the tumor size reached around 50 mm^2, mice began the presurgical treatment with p38 inhibitors or vehicle every other day. Once the tumor size reached ~200 mm^2, the primary tumors were resected. At 1 week after surgery, the animals began the treatment with these drugs every other day for 1 month. When animals displayed signs of respiratory stress or became moribund, they were killed and their lungs were collected and fixed in 4% PFA-PBS for H&E staining.

Immunofluorescence staining. The following antibodies were purchased and used: primary CD11b (BioLegend, Clone M1/70 cat. no. 101202, 1:100), Fibronectin (Abcam, cat. no. ab23750, 1:100), IFNAR1 (Sino Biological, cat. no. 50469-RP02, 1:100) and FAP (R&D, cat. no. AF3715, 1:100); and secondary antibodies: Alexa Fluor 488 Goat anti-Rat (Thermo Fisher Scientific, cat. no. A11006, 1:500) for CD11b, Alexa Fluor 488 Goat anti-Rabbit (Thermo Fisher Scientific, cat. no. A11070, 1:500) for fibronectin, Alexa Fluor 594 Goat anti-Rabbit (Thermo Fisher Scientific, cat. no. A11072, 1:500) for IFNAR1 and Alexa Fluor 488 Donkey anti-sheep (Thermo Fisher Scientific, cat. no. A11015, 1:500) for FAP. Immunofluorescence analyses were carried out as previously described[18]. The images were taken using the Olympus BX51 microscope. The quantification of immunofluorescence intensity was performed by ImageJ. Three sections were analyzed for each mouse and 6–10 fields in each section were quantified.

Flow cytometry analysis. Lung tissues were collected and washed with ice-cold PBS, and then cut into small pieces and incubated in dissociation solution with 2 mg ml^{-1} Collagenase II (MP Biomedicals), 1 mg ml^{-1} Collagenase IV (Roche) plus 100 µg ml^{-1} DNase I (Roche) solution for around 1 h with continuous agitation. The digestion mixture was passed through a 70-µm cell strainer and washed with PBS once. Then, 5 ml of RBC lysis buffer was added to cells and incubated for 5 min to lyse red blood cells. The cells were then washed with PBS once and resuspended with 1% BSA-PBS containing 1 mM EDTA. The isolated cells were incubated with anti-mouse CD16/CD32 antibody (BioLegend, Clone 93 cat. no. 101302, 1:50) for 15 min at room temperature to block nonspecific Fc receptor binding. Cells were then stained with cell surface markers anti-CD45-FITC (BioLegend, Clone 30-F11 cat. no. 103108, 1:500), anti-CD11b-APC (BioLegend, Clone M1/70 cat. no. 101212, 1:500), anti-Ly-6C-PE (BioLegend, Clone HK1.4 cat. no. 128007, 1:500), anti-Ly-6G-APC/Cy7 (BioLegend, clone 1A8 cat. no. 127624, 1:500), anti-CD45-APC/Cy7 (BioLegend, Clone 30-F11 cat. no. 103115, 1:500), anti-CD31-AF488 (BioLegend, Clone MEC13.3 cat. no. 102513, 1:500), anti-EpCAM (CD326)-PE/Cy7 (BioLegend, Clone G8.8 cat. no. 118216, 1:500), anti-PDGFRα (CD140a)-APC (BioLegend, Clone APA5 cat. no. 135908, 1:500) or anti-IFNAR1 (BioLegend, clone MAR1-5A3 cat. no. 127312, 1:500) and incubated on ice for 30 min. After washing with PBS, cells were resuspended with FACS buffer containing DAPI (1:2,000) for 10 min and acquired by LSRFortessa flow cytometry (BD Biosciences). Data were analyzed with FlowJo software (Tree Star).

For IFNAR1 and FAP staining on the isolated lung fibroblasts in vitro, cells were incubated with cell dissociation buffer (Gibco, cat. no. 13150-016) for 15 min at 37 °C and dispersed into a single-cell suspension. After washing with PBS, cells were stained with PE-conjugated anti-mouse IFNAR1 (BioLegend, clone MAR1-5A3 cat. no. 127312, 1:400) for 30 min, or biotinylated anti-mouse FAP (Dr. Puré laboratory home-made, 1:400) for 30 min, followed by a secondary streptavidin-APC (BioLegend, cat. no. 405207, 1:500) staining for another 30 min. Cells stained with PE-conjugated IgG-ctrl (BioLegend, clone MOPC-21 cat. no. 400112) or only secondary staining were used as negative control. After washing, cells were resuspended with FACS buffer containing DAPI (1:2,000) for 10 min and acquired on an LSRFortessa flow cytometer (BD Biosciences). Data were analyzed with FlowJo software (Tree Star).

Immunohistochemistry (IHC) staining. The IHC staining for phospho-p38 (Thr180/Tyr182) (Cell Signaling Technology, Clone 12F8 cat. no. 4631S, 1:400) of paraffin-embedded lung tissue sections was performed by the Histology Core at the School of Veterinary Medicine, University of Pennsylvania. The IHC score was assessed blindly by two pathologists who calculated both the percentage of stained cells and the intensity of staining as follows: the proportion of positive cells was estimated and given a percentage score on a scale from 1 to 6 (1, 1–10%; 2, 11–20%; 3, 21–40%; 4, 41–60%; 5, 61–80%; and 6, 81–100%). The average intensity of the positively stained cells was given an intensity score from 0 to 3 (0, no staining; 1, weak; 2, moderate; and 3, strong staining). The final IHC score was then calculated by multiplying the percentage score by the intensity score to yield a minimum value of 0 and a maximum value of 18.

Ex vivo immunosuppression assay. Granulocytes (Ly-6G$^+$) were purified from the lungs of mice that were administered with B16F10 TCM or from the spleens of MC38 tumor-bearing mice using MACS Separation kit (Miltenyi Biotec). Isolated granulocyte cells (1×10^5) were incubated with OT-1 WT splenocytes at different ratios of 1:1, 1:2 and 1:4. The mixed cells were co-cultured in 96-well plates with SIINFEKL (0.5 ng µl^{-1}) peptide stimulation for 48 h, and then ^{3}H thymidine (PerkinElmer) was added (1 µl per well for 24 h). The radioactivity of samples was counted with a TopCount NXT instrument (PerkinElmer) as previously described[59].

Quantitative PCR with reverse transcription. Total RNA was extracted using Trizol reagent (Invitrogen). The High-Capacity RNA-to-cDNA Kit (Applied Biosystems) was used to make complementary DNA. Real-time PCR was performed using SYBR Green Master Mix reagents (Applied Biosystems). The expression of each gene was calculated based on the cycle threshold, set within the linear range of DNA amplification. The relative expression

Fig. 8 | p38α deficiency specifically in fibroblasts attenuates lung metastasis and p38 inhibitors show efficient adjuvant therapeutic effects. a, Representative lung images and the corresponding H&E-stained lung sections from the tamoxifen-treated *Ifnar1*$^{fl/fl}$*Col1a2-CreER*$^-$ (*Ifnar1*$^{fl/fl}$) and *Ifnar1*$^{fl/fl}$ *Col1a2CreER*$^+$ (*Ifnar1*$^{\Delta Fib}$, IFNAR1 knockout specific in fibroblasts) mice after intravenous injection with B16F10 tumor cells (2×10^5 per mouse). Scale bar, 1 mm. Similar results were obtained from three independent experiments. **b**, Quantification of the number of metastatic lesions and total area in the lung tissues of *Ifnar1*$^{fl/fl}$ ($n=8$) and *Ifnar1*$^{\Delta Fib}$ ($n=7$) mice after B16F10 tumor cell injection as shown in **a**. Data are shown as mean ± s.e.m. Two-tailed unpaired *t*-test was performed for the comparison. **c**, Representative lung images and the corresponding H&E-stained lung sections from the tamoxifen-treated B16F10 tumor-bearing *Mapk14*$^{fl/fl}$ and *Mapk14*$^{\Delta Fib}$ mice after primary tumor removal at equivalent size (~200 mm^2). Scale bar, 1 mm. Similar results were obtained from three independent experiments. **d**, Quantification of the number of metastatic lesions and total area in the lung tissues of *Mapk14*$^{fl/fl}$ ($n=11$) and *Mapk14*$^{\Delta Fib}$ mice ($n=10$) after surgery as shown in **c**. Data are shown as mean ± s.e.m. Two-tailed unpaired *t*-test was performed for the comparison. **e**, Kaplan–Meier analysis of survival of B16F10 tumor-bearing *Mapk14*$^{fl/fl}$ ($n=13$) and *Mapk14*$^{\Delta Fib}$ ($n=11$) mice after surgery by log-rank test. **f**, Schematic illustration for analysis of the effect of p38 inhibitors ralimetinib (LY) or SB203580 (SB) as neoadjuvant/adjuvant therapeutic agents. **g**, Representative lung images and the corresponding H&E-stained lung sections in the mice after surgery as described in **f**. Scale bar, 1 mm. Similar results were obtained from three independent experiments. **h**, Quantification of the number of metastatic lesions and total area in the lung tissues of the mice after surgery as shown in **g**. Data are shown as mean ± s.e.m. ($n=8$ mice in Vehicle group, $n=10$ mice in LY group, $n=6$ mice in SB group). Two-tailed unpaired *t*-test was performed for the comparison. **i**, Kaplan–Meier analysis of survival of B16F10 tumor-bearing mice after surgery as described in **f** by log-rank test ($n=9$ mice in Vehicle and LY groups, $n=7$ mice in SB group). **j**, A model highlighting the key role of p38α kinase and downstream activation of FAP in the generation of the pre-metastatic niche in lung.

was calculated by the cycle threshold method, with normalization of raw data to a housekeeping gene (*Gapdh*). The primer sequences are provided in Supplementary Table 1.

Purification of FAP ECD. The 6xHistidine-tagged FAP ECD recombinant protein was expressed in 293T cells and purified on an Ni-NTA agarose column (Qiagen, cat. no. 30210). Briefly, 293T cells expressing His-FAP ECD were expanded in T225 flasks at ~80% confluency (~1.5×10^6 cells). Cells were collected and resuspended in 90 ml of 293 SFM II (Invitrogen, cat. no. 11686029), and incubated at 37 °C and 8% CO_2 with vigorous shaking. Cells were collected, spun down and resuspended in 30 ml of fresh media every 2 d until the cells looked round and bright. Then, 15 ml of cells ($1.5–2 \times 10^6$ cells per ml) were added into the growth compartment and 975 ml of media into the nutrient compartment in the bioreactor flask after equilibrium by adding 25 ml media and incubation at 37 °C for 15 min. After 72 h,

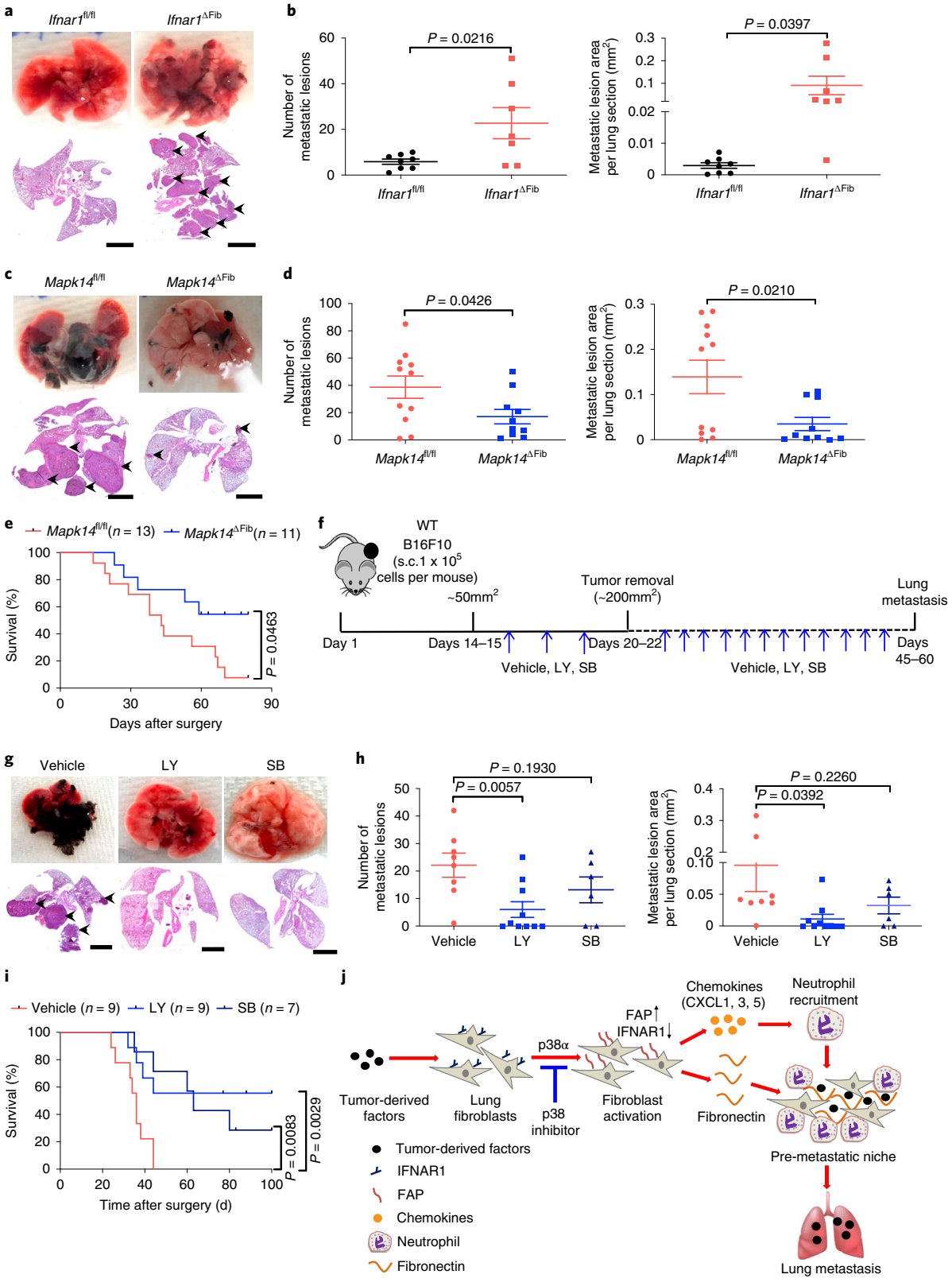

cells were collected and the supernatant was collected and subjected to dialysis against PBS. The dialyzed supernatant was incubated with washed Ni-Agarose slurry (Qiagen, cat. no. 30210) for 1 h at 4 °C with rocking. The incubation mix was added into a column followed by washing and elution with the corresponding buffer according to the manufacturers' instructions. Purity of this protein was assessed by SDS–PAGE followed by silver staining. FAP ECD was used in the in vitro assays at 0.3 μg ml^{-1}.

Chromatin immunoprecipitation (ChIP) analysis. ChIP analysis was performed in the lung fibroblasts treated with TCM or SFM for 12 h as previously described[29] using the following antibodies: H3K4me3 (Abcam, cat. no. ab8580), H3K9me3 (Abcam, cat. no. ab8898) and isotype control (Abcam, cat. no. ab171870). The following primers were used as described[31]: *Cxcl1* promoter region, 5′-CCTCTTCACATGCCTCCCTG-3′ (forward) and 5′-CGGGGATGGAAGCTTGTCTT-3′ (reverse); and *Actb* promoter region, 5′-CCTCTGGGTGTGGATGTCAC-3′ (forward) and 5′-TGTCCATTCAATCCAGGCCC-3′ (reverse).

RNA sequencing. WT and SA mice were intravenously injected with B16F10 TCM three times a week for 3 weeks. After injection, mice were euthanized. Lung tissues were collected and snap-frozen in liquid nitrogen. Total RNA of the lung tissue was isolated with miRNeasy mini kit (QIAGEN). Biotin-labeled antisense RNA preparations were obtained using TargetAmp-Nano Labeling Kit (Epicentre) as recommended by the manufacturer. Thereafter, 0.75 μg of antisense RNA was hybridized to Illumina Sentrix Mouse-6 v.1 BeadChips, which were scanned with an Illumina BeadStation 500 (both from Applied Biosystems Life Technologies). Data were collected with Illumina BeadStudio 3.1.1.0 software, and statistical analyses were conducted on the IlluminaGUI R-package. Gene set enrichment analysis was performed for overlap with curated datasets (C5, H) in MSigDB using the web interface available at http://www.broadinstitute.org/gsea/msigdb/index.jsp.

Statistics and reproducibility. All described results are representative of at least three independent experiments. Statistical analyses and the number of samples (n) were described in detail for each figure panel. No statistical method was used to predetermine sample size. Data were presented as average ± s.e.m. Statistical analysis was performed using Microsoft Excel (Microsoft) or GraphPad Prism 8 software (GraphPad). Two-tailed unpaired Student's t-test was used for the comparison between two groups. One-way analysis of variance (ANOVA) or two-way ANOVA followed by the Sidak's or Tukey's test was used for the multiple comparisons. Repeated-measures two-way ANOVA (mixed model) followed by the Sidak's multiple comparisons test was used for analysis of the tumor growth curve. The Kaplan–Meier curves were used to depict the survival function from lifetime data for mice and human patients; the log-rank test or Gehan–Breslow–Wilcoxon test was used to analyze the differences between the groups. Fisher's test was used for other comparisons. A value of $P < 0.05$ was considered significant. Mice that died within 24 h after surgery were assumed to have died because of procedure-related complications and were excluded from analysis. In western blot analysis of human blood leukocytes, three samples were excluded due to the low amount of protein (<1 μg). No other data were excluded. The experiments were not randomized, except that the mice were randomly grouped before treatment. Investigators were not blinded to allocation during the experiments and outcome assessments, except for the IHC score analysis.

Reporting Summary. Further information on research design is available in the Nature Research Reporting Summary linked to this article.

Data availability

RNA-sequencing data that support the findings of this study have been deposited in the Gene Expression Omnibus (GEO) under accession code GSE133781. Source data for Figs. 1–8 and Extended Data Figs. 1–8 have been provided as Source data files. All other data supporting the findings of this study are available from the corresponding author upon reasonable request.

Received: 24 June 2019; Accepted: 9 April 2020;
Published online: 25 May 2020

References

1. Joyce, J. A. & Pollard, J. W. Microenvironmental regulation of metastasis. *Nat. Rev. Cancer* **9**, 239–252 (2009).
2. Kaplan, R. N. et al. VEGFR1-positive haematopoietic bone marrow progenitors initiate the pre-metastatic niche. *Nature* **438**, 820–827 (2005).
3. Peinado, H., Lavotshkin, S. & Lyden, D. The secreted factors responsible for pre-metastatic niche formation: old sayings and new thoughts. *Semin. Cancer Biol.* **21**, 139–146 (2011).
4. Peinado, H. et al. Pre-metastatic niches: organ-specific homes for metastases. *Nat. Rev. Cancer* **17**, 302–317 (2017).
5. Francia, G., Cruz-Munoz, W., Man, S., Xu, P. & Kerbel, R. S. Mouse models of advanced spontaneous metastasis for experimental therapeutics. *Nat. Rev. Cancer* **11**, 135–141 (2011).
6. Woodard, P. K., Dehdashti, F. & Putman, C. E. Radiologic diagnosis of extrathoracic metastases to the lung. *Oncology* **12**, 431–438 (1998).
7. Kim, S. et al. Carcinoma-produced factors activate myeloid cells through TLR2 to stimulate metastasis. *Nature* **457**, 102–106 (2009).
8. Peinado, H. et al. Melanoma exosomes educate bone marrow progenitor cells toward a pro-metastatic phenotype through MET. *Nat. Med.* **18**, 883–891 (2012).
9. Liu, Y. et al. Tumor exosomal RNAs promote lung pre-metastatic niche formation by activating alveolar epithelial TLR3 to recruit neutrophils. *Cancer Cell* **30**, 243–256 (2016).
10. Erler, J. T. et al. Hypoxia-induced lysyl oxidase is a critical mediator of bone marrow cell recruitment to form the premetastatic niche. *Cancer Cell* **15**, 35–44 (2009).
11. Liu, Y. & Cao, X. Characteristics and significance of the pre-metastatic niche. *Cancer Cell* **30**, 668–681 (2016).
12. Arthur, J. S. & Ley, S. C. Mitogen-activated protein kinases in innate immunity. *Nat. Rev. Immunol.* **13**, 679–692 (2013).
13. Cuadrado, A. & Nebreda, A. R. Mechanisms and functions of p38 MAPK signalling. *Biochem. J.* **429**, 403–417 (2010).
14. Hui, L., Bakiri, L., Stepniak, E. & Wagner, E. F. p38α: a suppressor of cell proliferation and tumorigenesis. *Cell Cycle* **6**, 2429–2433 (2007).
15. Wagner, E. F. & Nebreda, A. R. Signal integration by JNK and p38 MAPK pathways in cancer development. *Nat. Rev. Cancer* **9**, 537–549 (2009).
16. Huangfu, W. C. et al. Inflammatory signaling compromises cell responses to interferon alpha. *Oncogene* **31**, 161–172 (2012).
17. Katlinskaya, Y. V. et al. Suppression of type I interferon signaling overcomes oncogene-induced senescence and mediates melanoma development and progression. *Cell Rep.* **15**, 171–180 (2016).
18. Ortiz, A. et al. An interferon-driven oxysterol-based defense against tumor-derived extracellular vesicles. *Cancer Cell* **35**, 33–45 e36 (2019).
19. Fearon, D. T. The carcinoma-associated fibroblast expressing fibroblast activation protein and escape from immune surveillance. *Cancer Immunol. Res.* **2**, 187–193 (2014).
20. Kraman, M. et al. Suppression of antitumor immunity by stromal cells expressing fibroblast activation protein-α. *Science* **330**, 827–830 (2010).
21. Pure, E. & Blomberg, R. Pro-tumorigenic roles of fibroblast activation protein in cancer: back to the basics. *Oncogene* **37**, 4343–4357 (2018).
22. Fidler, I. J. & Nicolson, G. L. Organ selectivity for implantation survival and growth of B16 melanoma variant tumor lines. *J. Natl Cancer Inst.* **57**, 1199–1202 (1976).
23. Bhattacharya, S. et al. Triggering ubiquitination of IFNAR1 protects tissues from inflammatory injury. *EMBO Mol. Med.* **6**, 384–397 (2014).
24. Bhattacharya, S. et al. Role of p38 protein kinase in the ligand-independent ubiquitination and down-regulation of the IFNAR1 chain of type I interferon receptor. *J. Biol. Chem.* **286**, 22069–22076 (2011).
25. Tcyganov, E., Mastio, J., Chen, E. & Gabrilovich, D. I. Plasticity of myeloid-derived suppressor cells in cancer. *Curr. Opin. Immunol.* **51**, 76–82 (2018).
26. Zhou, J., Nefedova, Y., Lei, A. & Gabrilovich, D. Neutrophils and PMN-MDSC: their biological role and interaction with stromal cells. *Semin. Immunol.* **35**, 19–28 (2018).
27. Andzinski, L. et al. Type I IFNs induce anti-tumor polarization of tumor associated neutrophils in mice and human. *Int. J. Cancer* **138**, 1982–1993 (2016).
28. Kumar, V. et al. Cancer-associated fibroblasts neutralize the anti-tumor effect of CSF1 receptor blockade by inducing PMN-MDSC infiltration of tumors. *Cancer Cell* **32**, 654–668 e655 (2017).
29. Li, J. et al. Tumor cell-intrinsic factors underlie heterogeneity of immune cell infiltration and response to immunotherapy. *Immunity* **49**, 178–193 e177 (2018).
30. Kroetz, D. N. et al. Type I interferon induced epigenetic regulation of macrophages suppresses innate and adaptive immunity in acute respiratory viral infection. *PLoS Pathog.* **11**, e1005338 (2015).
31. Schliehe, C. et al. The methyltransferase Setdb2 mediates virus-induced susceptibility to bacterial superinfection. *Nat. Immunol.* **16**, 67–74 (2015).
32. Hoye, A. M. & Erler, J. T. Structural ECM components in the premetastatic and metastatic niche. *Am. J. Physiol. Cell Physiol.* **310**, C955–C967 (2016).
33. Roberts, E. W. et al. Depletion of stromal cells expressing fibroblast activation protein-α from skeletal muscle and bone marrow results in cachexia and anemia. *J. Exp. Med.* **210**, 1137–1151 (2013).
34. Santos, A. M., Jung, J., Aziz, N., Kissil, J. L. & Pure, E. Targeting fibroblast activation protein inhibits tumor stromagenesis and growth in mice. *J. Clin. Invest.* **119**, 3613–3625 (2009).
35. Alspach, E. et al. p38MAPK plays a crucial role in stromal-mediated tumorigenesis. *Cancer Discov.* **4**, 716–729 (2014).
36. Brichkina, A. et al. p38MAPK builds a hyaluronan cancer niche to drive lung tumorigenesis. *Genes Dev.* **30**, 2623–2636 (2016).

37. Matsuo, Y. et al. Involvement of p38α mitogen-activated protein kinase in lung metastasis of tumor cells. *J. Biol. Chem.* **281**, 36767–36775 (2006).
38. Chen, X. W. et al. CYP4A in tumor-associated macrophages promotes pre-metastatic niche formation and metastasis. *Oncogene* **36**, 5045–5057 (2017).
39. Correa, D., Somoza, R. A., Lin, P., Schiemann, W. P. & Caplan, A. I. Mesenchymal stem cells regulate melanoma cancer cells extravasation to bone and liver at their perivascular niche. *Int. J. Cancer* **138**, 417–427 (2016).
40. Murgai, M. et al. KLF4-dependent perivascular cell plasticity mediates pre-metastatic niche formation and metastasis. *Nat. Med.* **23**, 1176–1190 (2017).
41. van Deventer, H. W., Palmieri, D. A., Wu, Q. P., McCook, E. C. & Serody, J. S. Circulating fibrocytes prepare the lung for cancer metastasis by recruiting Ly-6C$^+$ monocytes via CCL2. *J. Immunol.* **190**, 4861–4867 (2013).
42. Zheng, H. et al. Vascular endothelial growth factor-induced elimination of the type 1 interferon receptor is required for efficient angiogenesis. *Blood* **118**, 4003–4006 (2011).
43. Qian, J. et al. Pathogen recognition receptor signaling accelerates phosphorylation-dependent degradation of IFNAR1. *PLoS Pathog.* **7**, e1002065 (2011).
44. Kalluri, R. The biology and function of exosomes in cancer. *J. Clin. Invest.* **126**, 1208–1215 (2016).
45. Lobb, R. J., Lima, L. G. & Moller, A. Exosomes: key mediators of metastasis and pre-metastatic niche formation. *Semin. Cell Dev. Biol.* **67**, 3–10 (2017).
46. Sceneay, J., Smyth, M. J. & Moller, A. The pre-metastatic niche: finding common ground. *Cancer Metast. Rev.* **32**, 449–464 (2013).
47. Rautela, J. et al. Loss of host type-I IFN signaling accelerates metastasis and impairs NK-cell antitumor function in multiple models of breast cancer. *Cancer Immunol. Res.* **3**, 1207–1217 (2015).
48. Feig, C. et al. Targeting CXCL12 from FAP-expressing carcinoma-associated fibroblasts synergizes with anti-PD-L1 immunotherapy in pancreatic cancer. *Proc. Natl Acad. Sci. USA* **110**, 20212–20217 (2013).
49. Ohlund, D., Elyada, E. & Tuveson, D. Fibroblast heterogeneity in the cancer wound. *J. Exp. Med.* **211**, 1503–1523 (2014).
50. Ohlund, D. et al. Distinct populations of inflammatory fibroblasts and myofibroblasts in pancreatic cancer. *J. Exp. Med.* **214**, 579–596 (2017).
51. Choudhury, S. R. et al. Dipeptidase-1 is an adhesion receptor for neutrophil recruitment in lungs and liver. *Cell* **178**, 1205–1221 e1217 (2019).
52. Lo, A. et al. Fibroblast activation protein augments progression and metastasis of pancreatic ductal adenocarcinoma. *JCI Insight* **2**, pii: 92232 (2017).
53. Albrengues, J. et al. Neutrophil extracellular traps produced during inflammation awaken dormant cancer cells in mice. *Science* **361**, eaao4227 (2018).
54. Steeg, P. S. Targeting metastasis. *Nat. Rev. Cancer* **16**, 201–218 (2016).
55. Bragado, P. et al. TGF-β2 dictates disseminated tumour cell fate in target organs through TGF-β-RIII and p38α/β signalling. *Nat. Cell Biol.* **15**, 1351–1361 (2013).
56. Wu, X. et al. Ubiquitin-conjugating enzyme Ubc13 controls breast cancer metastasis through a TAK1-p38 MAP kinase cascade. *Proc. Natl Acad. Sci. USA* **111**, 13870–13875 (2014).
57. Katlinski, K. V. et al. Inactivation of interferon receptor promotes the establishment of immune privileged tumor microenvironment. *Cancer Cell* **31**, 194–207 (2017).
58. Patnaik, A. et al. A first-in-human phase I study of the oral p38 MAPK inhibitor, ralimetinib (LY2228820 dimesylate), in patients with advanced cancer. *Clin. Cancer Res.* **22**, 1095–1102 (2016).
59. Kumar, V. et al. CD45 phosphatase inhibits STAT3 transcription factor activity in myeloid cells and promotes tumor-associated macrophage differentiation. *Immunity* **44**, 303–315 (2016).

Acknowledgements

This work was supported by the PA Department of Health 2017 Health Research Formula Fund (to S.Y.F.); by the NIH/NCI R01 grant no. CA216936 (to S.Y.F. and D.I.G.), grant no. CA092900 (to S.Y.F.), grant no. CA229803 (to B.Z.S) and grant no. P01 CA165997 (to C.K., J.A.D. and S.Y.F.); as well as by additional support from grant no. F32 CA206431 (to A.O.), grant no. T32 CA009140 (to K.V.K.) and grant no. CA121973 (to J.M.K.). We thank Y. Wang, S. Weiss and E. Brown for the reagents, and A. Gamero (Temple University) and the members of the Gabrilovich, Fuchs, Diehl and Koumenis laboratories for critical suggestions.

Author contributions

S.Y.F. and J.G. conceived the study and designed the research. J.G. performed most of the experiments with the help of F.Z., C.C., A.O. and H.Z. and interpreted the data. K.V.K. and D.P.B performed RNA-sequencing data analysis. K.A.-T. performed the immunosuppression assay. J.L. performed ChIP experiments. C.S. and J.M.K. provided human samples and helped with analysis. B.E.S., A.C.W., T.W.M., L.T. and E.P. developed key reagents and provided technical assistance. S.Y.F. and J.G. wrote the manuscript. B.Z.S., D.I.G., E.P., C.K., S.W.R. and J.A.D. helped to design the research, discussed the results and commented on the manuscript.

Competing interests

The authors declare no competing interests.

Additional information

Extended data is available for this paper at https://doi.org/10.1038/s43018-020-0064-0.

Supplementary information is available for this paper at https://doi.org/10.1038/s43018-020-0064-0.

Correspondence and requests for materials should be addressed to S.Y.F.

Reprints and permissions information is available at www.nature.com/reprints.

Publisher's note Springer Nature remains neutral with regard to jurisdictional claims in published maps and institutional affiliations.

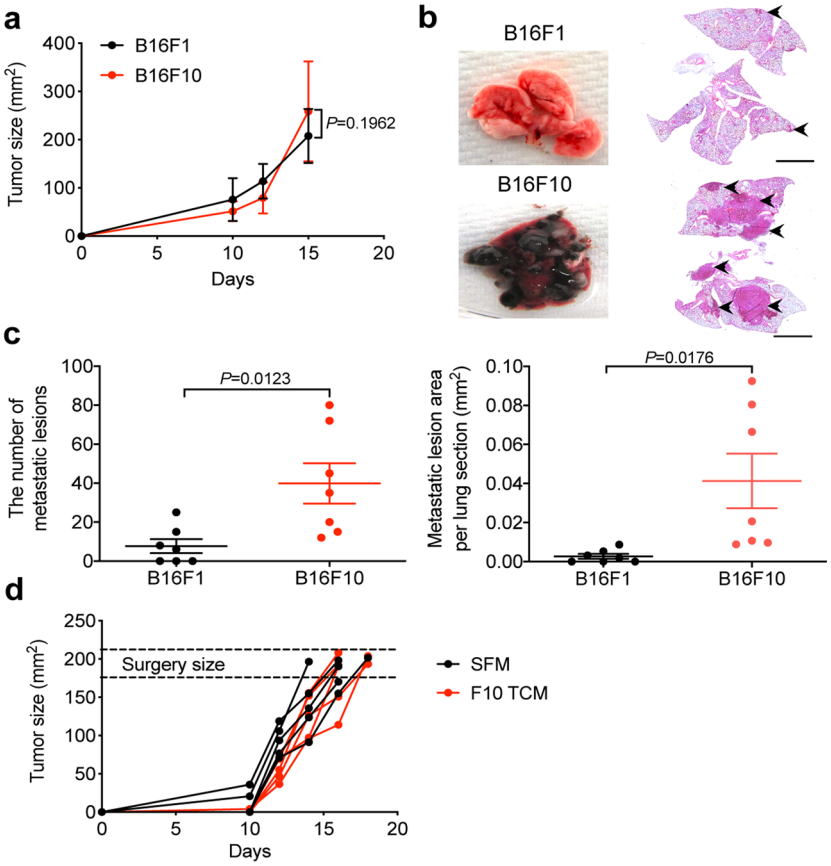

Extended Data Fig. 1 | Characterization of the metastasis in the lung tissues of B16F1 and B16F10 tumor bearing mice. a, The primary tumor growth in WT mice s.c injected with 1×10^5 B16F1 or B16F10 tumor cells prior to surgery at equivalent tumor size (~200 mm^2). Data shown as mean ± SEM (n = 7 mice per group). Repeated-measure two-way ANOVA and Sidak's multiple comparisons test were performed. **b**, A representative lung images and the corresponding H&E stained lung sections in the B16F1 and B16F10 tumor bearing mice after surgery. Scale bar: 1 mm. This experiment was repeated three times independently with similar results. **c**, Quantification of the number of metastatic lesions and total area in the lung tissues from B16F1 and B16F10 tumor bearing mice after surgery as shown in **b**. Data shown as mean ± SEM (n = 7 mice per group). Two-tailed Unpaired t test was performed for the comparison. **d**, The primary tumor growth in the B16F1 tumor bearing mice treated with SFM or B16F10 TCM prior to surgery (100 µl every other day until primary tumor removal upon reaching the size ~200 mm^2). n = 5 mice per group.

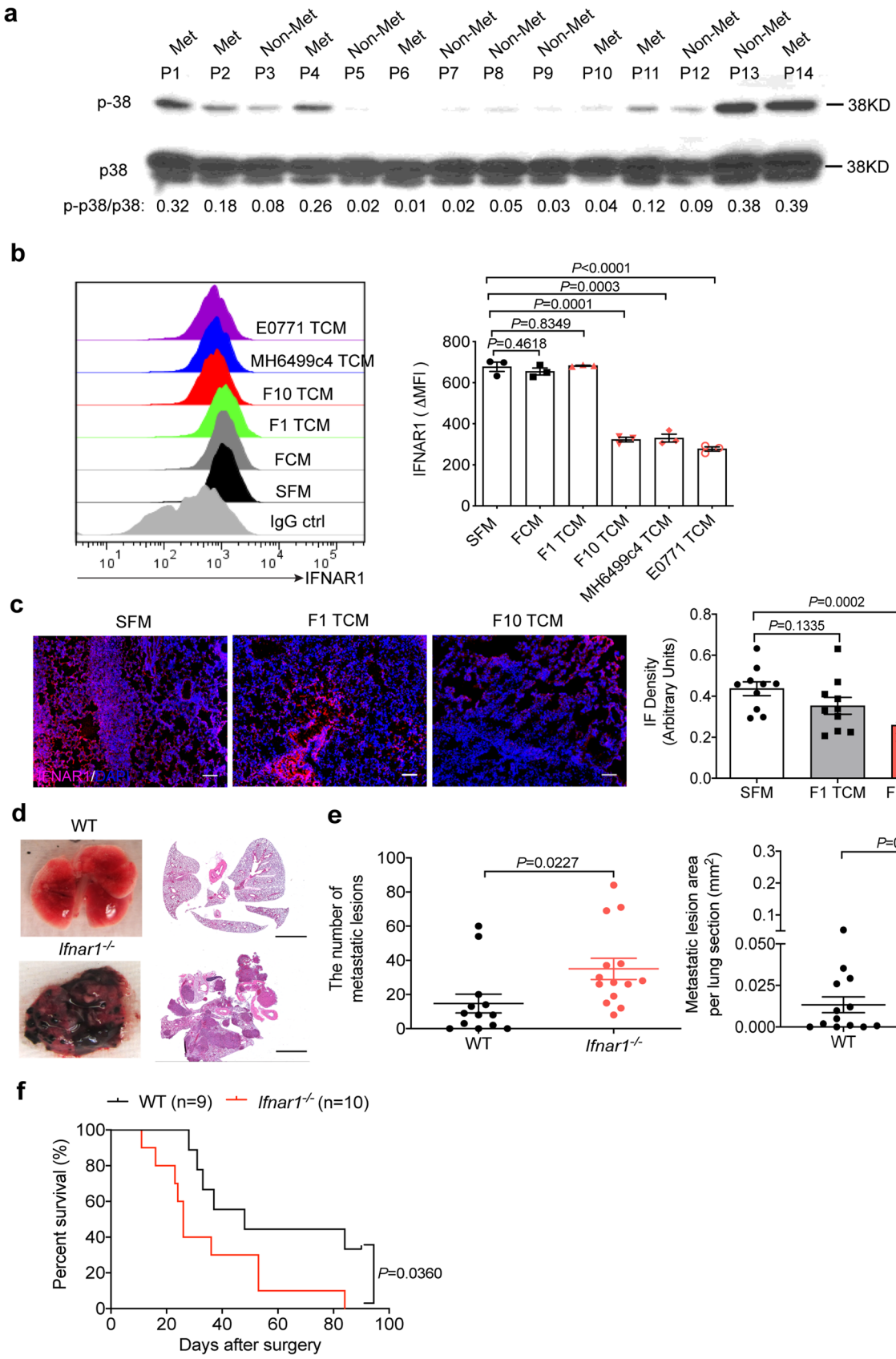

Extended Data Fig. 2 | See next page for caption.

Extended Data Fig. 2 | Tumor derived factors induce p38 activation and IFNAR1 downregulation. a, A representative western blot analysis of p-p38 and total p38 in the leukocytes isolated from the peripheral blood of melanoma patients with metastasis (Met) and without metastasis (Non-Met). The ratio of p-38 to p38 was shown at bottom for each patient. This experiment was repeated three times independently with similar results. **b**, A representative flow cytometry histogram (left) and the quantification of surface IFNAR1 level (right) in WT lung fibroblasts 2 hr after SFM, conditioned media from normal lung fibroblasts (FCM), or TCM from different tumor cells including B16F1, B16F10, MH6499c4, and E0771. Quantitative data shown as mean ± SEM (n = 3 biologically independent samples). Two- tailed Unpaired t test was performed for the comparisons between two groups. **c**, A representative immunofluorescence staining of IFNAR1 (left) and the quantification of IFNAR1 level (right) in the lung tissues from WT mice treated with SFM, B16F1 TCM or B16F10 TCM (100 µl i.v., 3x per week for 3 weeks). Scale bar: 100 µm. Quantitative data shown as mean ± SEM (n = 10 mice per group). Two-tailed Unpaired t test was performed for the comparisons between two groups. **d**, Representative lung images and the corresponding H&E-stained lung sections in WT and *Ifnar1*$^{-/-}$ B16F1 tumor bearing mice after surgery. Lung metastases were analyzed around 30–60 days after primary tumor removal upon reaching the size ~200mm^2. Scale bar: 1 mm. This experiment was repeated three times independently with similar results. **e**, Quantification of the number of metastatic lesions and total area in the lung tissues from WT (n = 13 mice) and *Ifnar1*$^{-/-}$ (n = 14 mice) B16F1 tumor bearing mice after surgery. Data shown as mean ± SEM. Two-tailed Unpaired t test was performed for the comparison. **f**, Kaplan-Meier analysis of survival of WT (n = 9 mice) and *Ifnar1*$^{-/-}$ (n = 10 mice) B16F1 tumor bearing mice after surgery by Log-rank test.

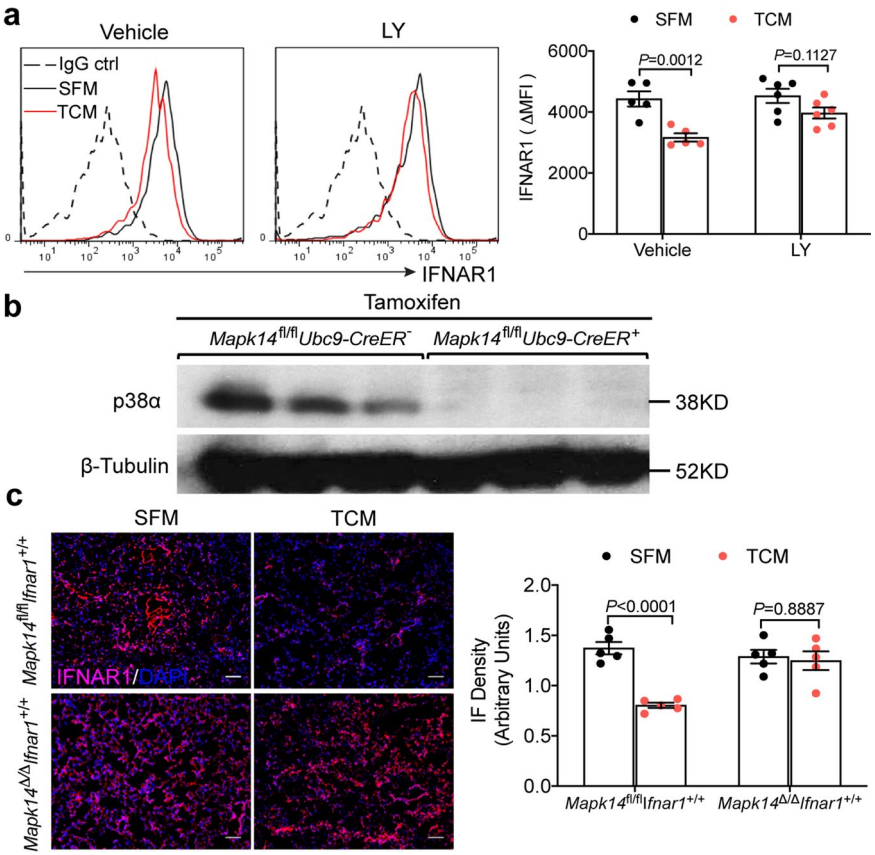

Extended Data Fig. 3 | p38α inhibition or gene deletion impede tumor derived factors-induced downregulation of IFNAR1. a, A representative flow cytometry analysis (left) and the quantification of surface IFNAR1 level (right) in WT lung fibroblasts pretreated with vehicle (DMSO) or p38 inhibitor Ralimetinib (LY2228820, 4 μM for 2 hr) followed by SFM, or B16F10 TCM treatment for additional 2 hr. Quantitative data shown as mean ± SEM (n = 5,and n = 6 biologically independent samples in Vehicle and LY treated group). Two-way ANOVA and Sidak's multiple comparisons test were performed. **b**, A representative western blot analysis of total p38α protein level in the lung tissues of *Mapk14*$^{fl/fl}$ *Ubc9-CreER*$^{-}$ and *Mapk14*$^{fl/fl}$*Ubc9-CreER*$^{+}$ mice after tamoxifen treatment. Similar results were obtained from three independent experiments. **c**, A representative immunofluorescence staining of IFNAR1 (left) and the quantification of IFNAR1 level (right) in the lung tissues from *Mapk14* competent mice (*Mapk14*$^{fl/fl}$) and *Mapk14* deleted mice (*Mapk14*$^{\Delta/\Delta}$) treated with SFM or B16F10 TCM (100 μl i.v., 3x per week for 3 weeks). Scale bar: 100 μm. Quantitative data shown as mean ± SEM (n = 5 mice per group). Two-way ANOVA and Sidak's multiple comparisons test were performed.

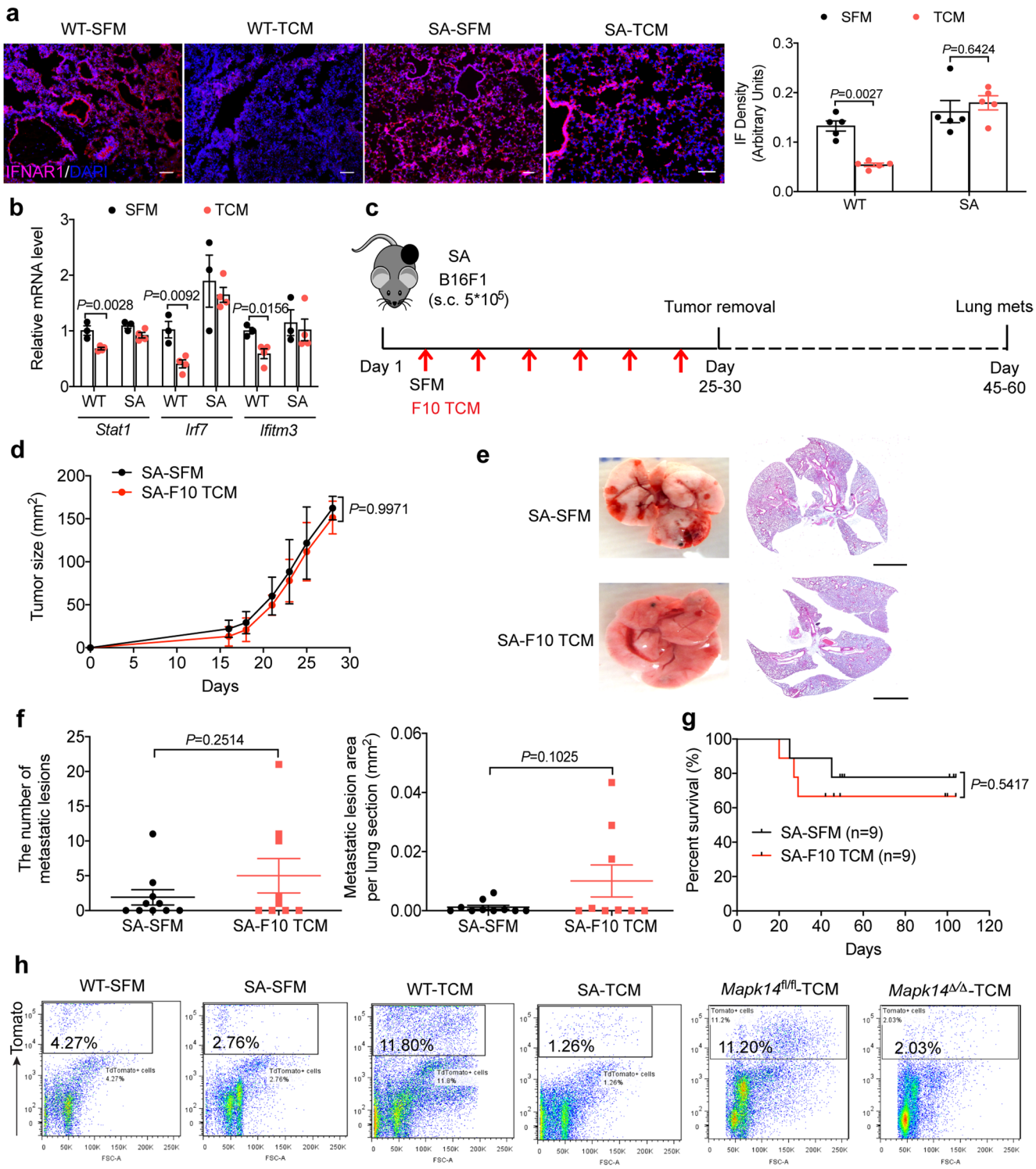

Extended Data Fig. 4 | See next page for caption.

Extended Data Fig. 4 | p38α-mediated IFNAR1 downregulation drives the formation of pre-metastatic niche in the lungs. a, A representative immunofluorescence staining of IFNAR1 (left) and the quantification of IFNAR1 level (right) in the lung tissues from WT and SA mice treated with SFM or B16F10 TCM. Scale bar: 100 μm. Quantitative data shown as mean ± SEM (n = 5 mice per group). Two-way ANOVA and Sidak's multiple comparisons test were performed. **b**, qPCR analysis of mRNA levels of indicated interferon stimulated genes in the lung tissues of WT and SA mice treated with SFM or B16F10 TCM. Data shown as mean ± SEM (n = 3, n = 4 mice in SFM and TCM treated group respectively). Two-way ANOVA and Tukey's multiple comparisons test were performed. **c**, Schematic illustration for analysis of the lung metastasis in the B16F1 tumor bearing SA mice treated with SFM or B16F10 TCM (100 μl i.v. every other day until primary tumor removal upon reaching the size ~200 mm^2). **d**, The primary tumor growth of B16F1 in SA mice treated with SFM or B16F10 TCM prior to surgery. Data shown as mean ± SEM (n = 4 mice per group). Repeated-measure two-way ANOVA and Sidak's multiple comparisons test were performed. **e**, Representative lung images and the corresponding H&E-stained lung sections of indicated mice as described in **c**. Scale bar: 1 mm. Similar results were obtained from three independent experiments. **f**, Quantification of the number of metastatic lesions and total area in the lung tissues from B16F1 tumor bearing SA mice treated with SFM (n = 10 mice) or B16F10 TCM (n = 9 mice) after surgery. Data shown as mean ± SEM. Two-tailed Unpaired t test was performed for the comparison. **g**, Kaplan-Meier analysis of survival of B16F1 tumor bearing SA mice treated with SFM (n = 9 mice) or B16F10 TCM (n = 9 mice) after surgery by Log-rank test. **h**, Representative flow cytometry analysis of tumor cells ($TdTomato^+$) in the lung tissues of WT, SA, and tamoxifen treated-*Mapk14*$^{fl/fl}$*Ubc9-CreER*$^-$ (*Mapk14*$^{fl/fl}$) and *Mapk14*$^{fl/fl}$*Ubc9-CreER*$^+$ (*Mapk14*$^{\Delta/\Delta}$) mice pretreated with SFM or B16F10 TCM followed by intravenous injection of $5*10^5$ B16F10-TdTomato cells. Similar results were obtained from three independent experiments.

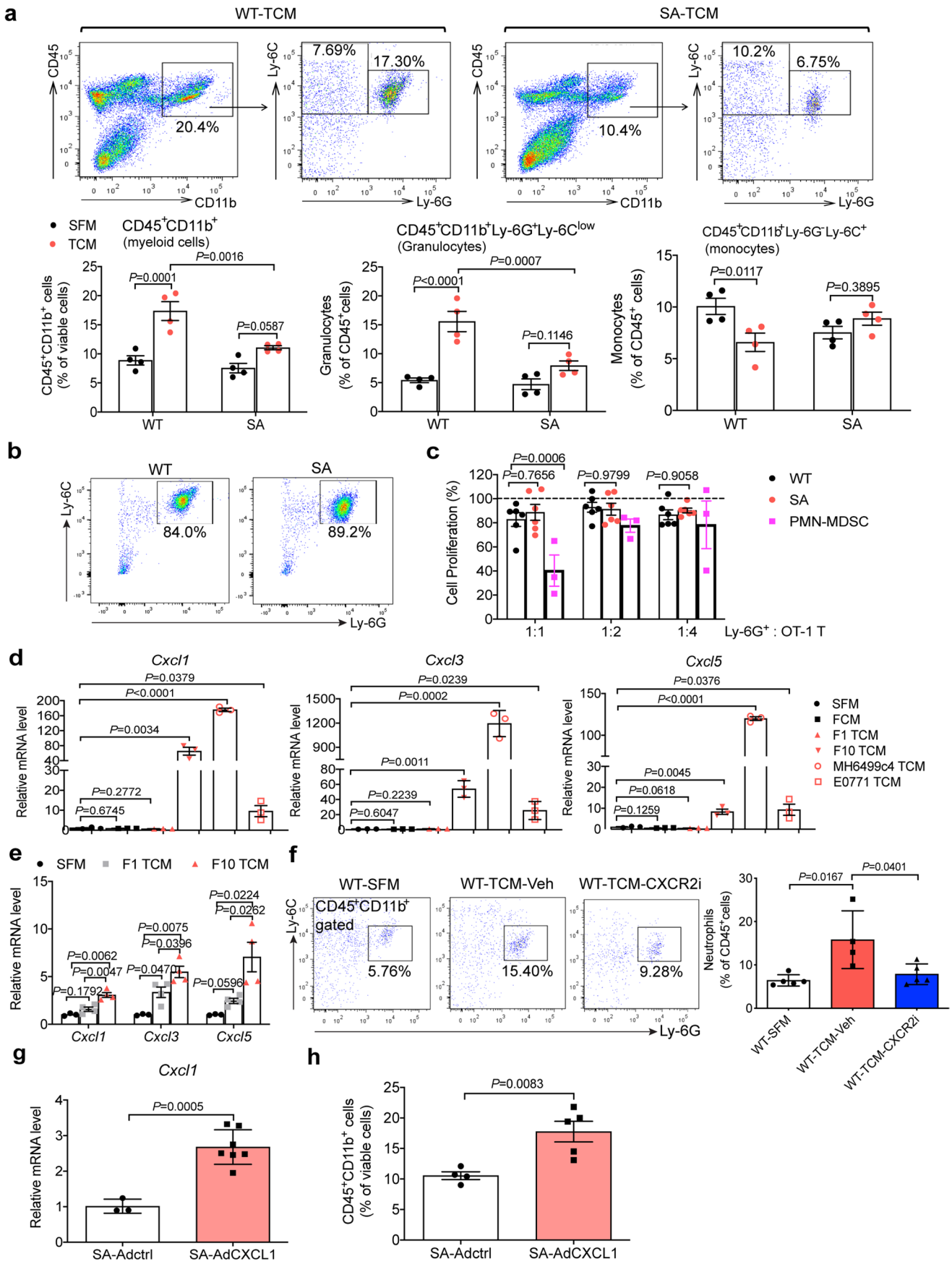

Extended Data Fig. 5 | See next page for caption.

Extended Data Fig. 5 | p38α-mediated IFNAR1 downregulation induces CXCL1/CXCL3/CXCL5-CXCR2 axis which is critical for the neutrophil recruitment. a, Representative flow cytometry analysis of myeloid cell subpopulations (above) and the quantification of these cell subpopulations (below) in the lung tissues of WT and SA mice treated with SFM or B16F10 TCM. Quantitative data shown as mean ± SEM (n = 4 mice per group). Two-way ANOVA and Sidak's multiple comparisons test were performed. **b**, Representative flow cytometry analysis of the purity of the isolated granulocytes from lung tissues of WT and SA mice treated with B16F10 TCM. Similar results were obtained from three independent experiments. **c**, Antigen-specific proliferation of $CD8^+$ T cells in the presence of isolated granulocytes ($Ly\text{-}6G^+$) from the lung tissues of WT and SA mice treated with B16F10 TCM at a ratio of 1:1, 1:2 or 1:4 measured as the uptake of ^3H thymidine and presented relative to that in the absence of granulocytes which set as 100%. Splenic PMN-MDSC isolated from MC38 tumor-bearing mice served as a positive control for the suppression. Data shown as mean ± SEM (n = 6 mice for WT and SA group, n = 3 mice for PMN-MDSC). Two-way ANOVA and Sidak's multiple comparisons test were performed. **d**, qPCR analysis of mRNA levels of the indicated chemokines in WT lung fibroblasts 6 hr after SFM, conditioned media from normal lung fibroblasts (FCM), or TCM from different tumor cells including B16F1, B16F10, MH6499c4, and E0771. Data shown as mean ± SEM (n = 3 biologically independent samples). Two-tailed Unpaired t test was performed for the comparisons between two groups. **e**, qPCR analysis of mRNA levels of the indicated chemokines in the lung tissues of WT mice treated with SFM (n = 3 mice), B16F1 TCM (n = 4 mice) or B16F10 TCM (n = 4 mice). Data shown as mean ± SEM. Two-way ANOVA and Tukey's multiple comparisons test were performed. **f**, Representative flow cytometry analysis (left) and the quantification of percent of neutrophils (right) in the lung tissues of WT mice treated with SFM (n = 5 mice), B16F10 TCM plus vehicle (n = 4 mice) or CXCR2 inhibitor (n = 5 mice). Quantitative data shown as mean ± SEM. Two-tailed Unpaired t test was performed for the comparisons between two groups. **g**, qPCR analysis of mRNA level of *Cxcl1* in the lung tissues of SA mice intranasally administered with control (n = 3 mice) or CXCL1 (n = 7 mice) expressing adenovirus. Data shown as mean ± SEM. Two-tailed Unpaired t test was performed for the comparison. **h**, The percent of total myeloid cells in the lung tissues of SA mice intranasally administered with control (n = 4 mice) or CXCL1 (n = 5 mice) expressing adenovirus. Data shown as mean ± SEM. Two-tailed Unpaired t test was performed for the comparison.

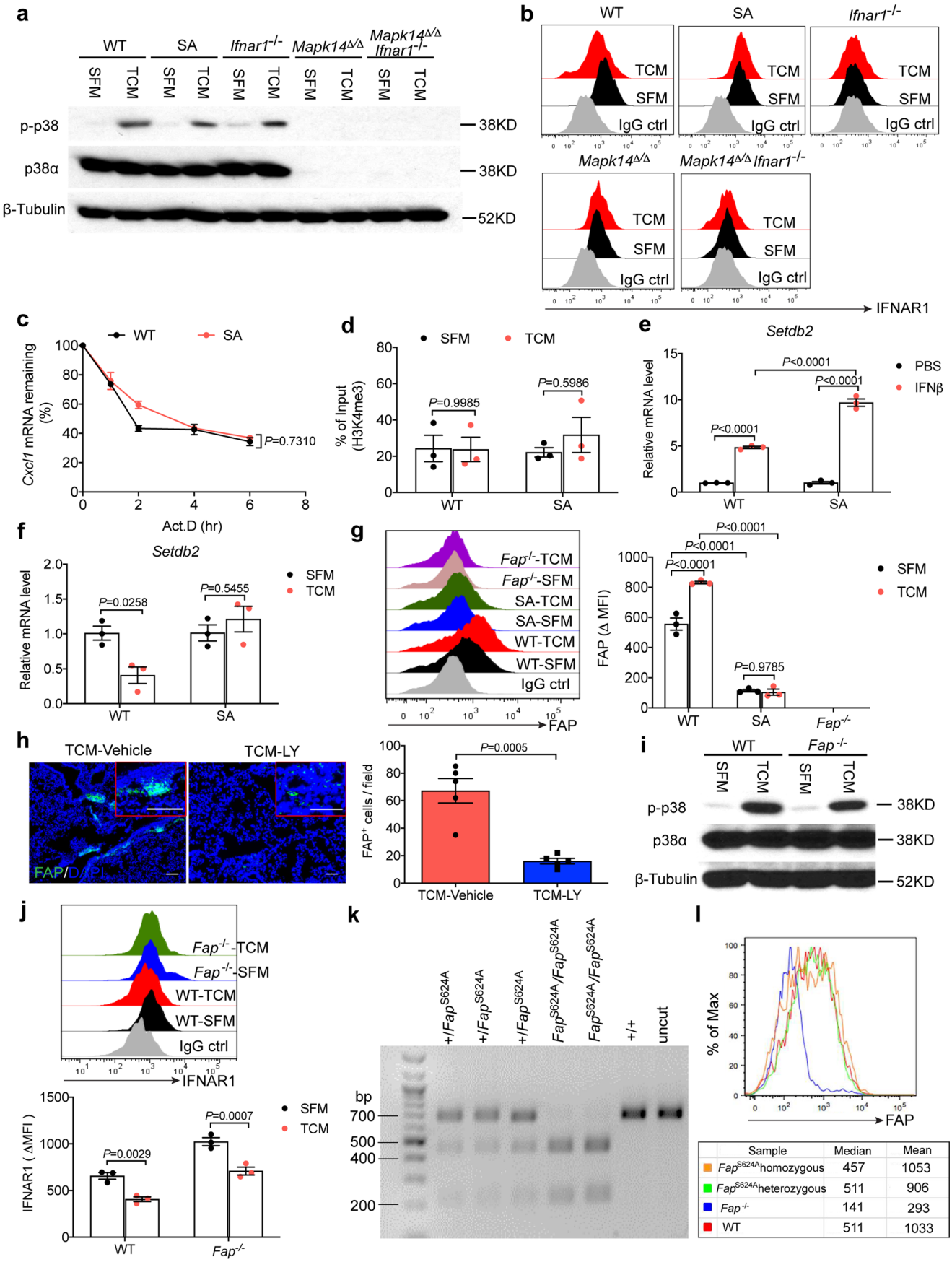

Extended Data Fig. 6 | See next page for caption.

Extended Data Fig. 6 | p38α-mediated IFNAR1 downregulation induces FAP expression. a, A representative western blot analysis of p-p38 and total p38 in the lung fibroblasts of WT, SA, *Ifnar1* null (*Ifnar1*$^{-/-}$), *Mapk14* deletion (*Mapk14*$^{\Delta/\Delta}$), *Mapk14* deletion along with *Ifnar1* null (*Mapk14*$^{\Delta/\Delta}$ *Ifnar1*$^{-/-}$) 1 hr after SFM or B16F10 TCM treatment in vitro. **b**, A representative flow cytometry analysis of surface IFNAR1 level in the lung fibroblasts of WT, SA, *Ifnar1*$^{-/-}$, *Mapk14*$^{\Delta/\Delta}$, *Mapk14*$^{\Delta/\Delta}$ *Ifnar1*$^{-/-}$ 2 hr after SFM or B16F10 TCM treatment in vitro. **c**, The decay of *Cxcl1* mRNA in WT and SA lung fibroblasts treated with SFM, or B16F10 TCM for 12 hr, then exposed to Actinomycin D (5 μg/ml) to terminate transcription. *Cxcl1* mRNA level was determined by qPCR. Data shown as mean ± SEM (n = 3 independent experiments). Repeated-measure two-way ANOVA and Sidak's multiple comparisons test were performed. **d**, ChIP analysis of H3K4me3 binding to the *Cxcl1* promoter in the isolated WT and SA lung fibroblasts treated with SFM or B16F10 TCM for 12 hr. Data shown as mean ± SEM (n = 3 independent experiments). Two-way ANOVA and Sidak's multiple comparisons test were performed. **e**, The mRNA level of *Setdb2* in WT and SA lung fibroblasts treated with PBS or murine IFNβ (1000 IU/ml) for 4 hr. Data shown as mean ± SEM (n = 3 biologically independent samples). Two-way ANOVA and Sidak's multiple comparisons test were performed. **f**, The mRNA level of *Setdb2* in WT and SA lung fibroblasts treated with SFM or B16F10 TCM for 4 hr. Data shown as mean ± SEM (n = 3 biologically independent samples). Two-way ANOVA and Sidak's multiple comparisons test were performed. **g**, A representative flow cytometry histogram (left) and the quantification of FAP expression (right) in the lung fibroblasts of WT, SA, and *Fap*$^{-/-}$ 24 hr after SFM or B16F10 TCM treatment. Quantitative data shown as mean ± SEM (n = 3 biologically independent samples). Two-way ANOVA and Sidak's multiple comparisons test were performed. **h**, A representative immunofluorescence staining of FAP (left) and the quantification of FAP^{+} cells (right) in the lung tissues from WT mice treated with B16F10 TCM plus vehicle or p38 inhibitor LY2228820. Scale bar: 100 μm. Quantitative data shown as mean ± SEM (n = 5 mice per group). Two-tailed Unpaired t test was performed for the comparison. **i**, A representative western blot analysis of p-p38 and total p38 in the lung fibroblasts of WT and *Fap*$^{-/-}$ 1 hr after SFM or B16F10 TCM treatment in vitro. **j**, A representative flow cytometry histogram (above) and the quantification of surface IFNAR1 level (bottom) in the lung fibroblasts of WT and *Fap*$^{-/-}$ 2 hr after SFM or B16F10 TCM treatment in vitro. Quantitative data shown as mean ± SEM (n = 3 biologically independent samples). Two-way ANOVA and Sidak's multiple comparisons test were performed. **k**, Genotyping of *Fap*^{S624A} mutant mice. A 677 bp amplicon was amplified by PCR both in the wild-type and *Fap*^{S624A} knock-in mouse. The 1 bp change generated a Stu1 restriction site (AG**G** | CCT) only in the knock-in mice. The PCR products were cleaned up and then digested with Stu1 producing the cut size of 210 bp and 467 bp. **l**, A representative flow cytometry analysis of FAP levels in the adult dermal fibroblasts isolated from *Fap*$^{+/+}$, *Fap*$^{-/-}$, *Fap*$^{S624A/S624A}$ and *Fap*$^{S624A/+}$ mice. The experiments in **a**, **b**, **i**, **k**, **l** were repeated three times independently with similar results, and the results of one representative experiment are shown.

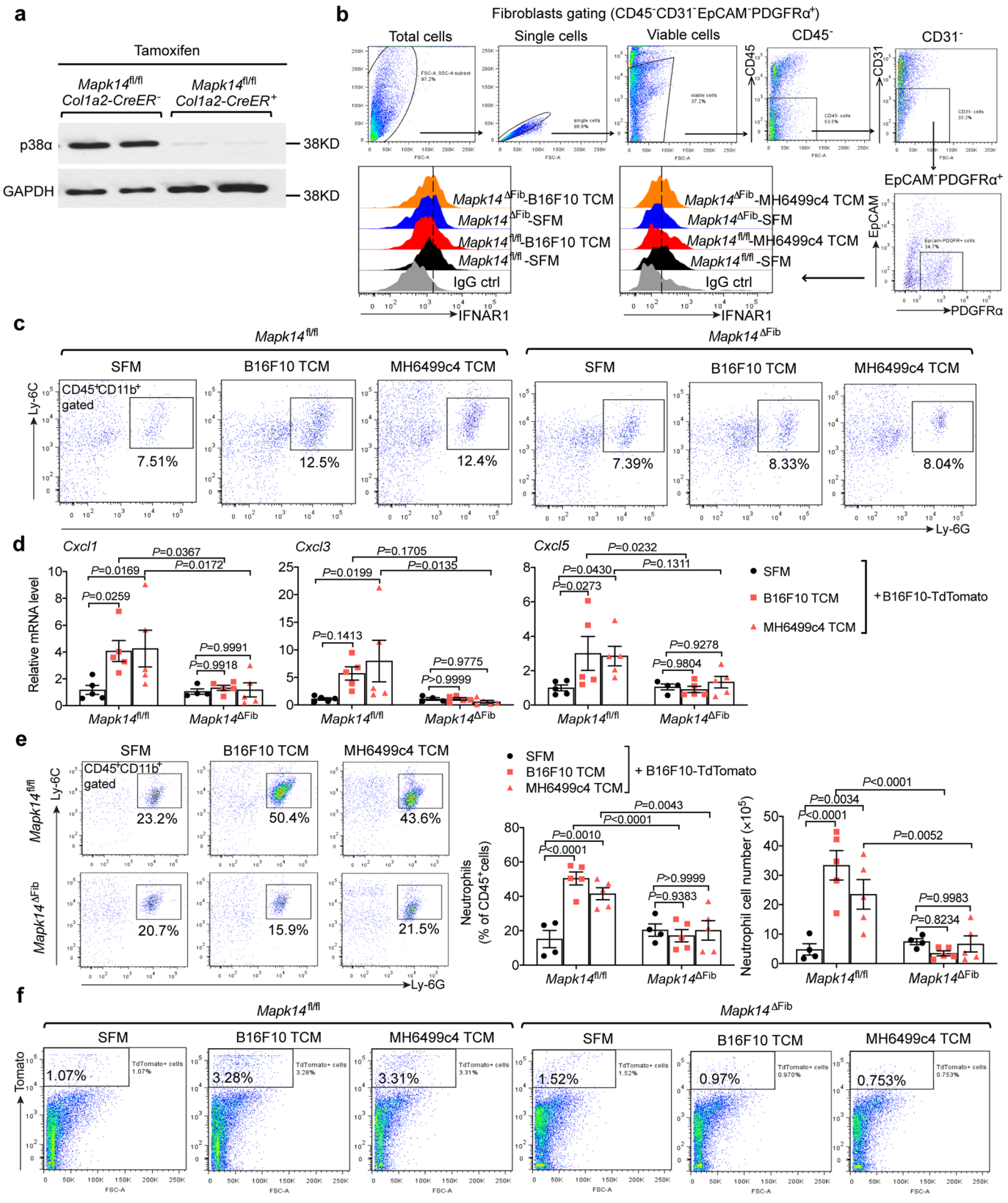

Extended Data Fig. 7 | See next page for caption.

Extended Data Fig. 7 | P38α expression in fibroblasts is critical for the generation of pre-metastatic niche. a, Representative western blot analysis of p38α protein level in the isolated lung fibroblasts from tamoxifen-treated *Mapk14*$^{fl/fl}$*Col1a2-CreER*$^{-}$ (*Mapk14*$^{fl/fl}$) and *Mapk14*$^{fl/fl}$*Col1a2-CreER*$^{+}$ (*Mapk14*$^{\Delta Fib}$, p38α knock out specific in fibroblasts) mice. **b**, A representative flow cytometry gating and histogram of IFNAR1 level in the lung fibroblasts of *Mapk14*$^{fl/fl}$ and *Mapk14*$^{\Delta Fib}$ mice injected with SFM, B16F10 TCM, or MH6499c4 TCM. **c**, Representative flow cytometry analysis of neutrophils in the lung tissues of *Mapk14*$^{fl/fl}$ and *Mapk14*$^{\Delta Fib}$ mice injected with SFM, B16F10 TCM, MH6499c4 TCM. **d**, qPCR analysis of the indicated chemokines in the lung tissues of *Mapk14*$^{fl/fl}$ and *Mapk14*$^{\Delta Fib}$ mice pretreated with SFM, B16F10 TCM, or MH6499c4 TCM followed by intravenous injection of 5*10^{5} B16F10-TdTomato cells. Data shown as mean ± SEM (n = 4 mice for SFM treated *Mapk14*$^{\Delta Fib}$ group, n = 5 mice for all the other groups). Two-way ANOVA and Tukey's multiple comparisons test were performed. **e**, Representative flow cytometry analysis (left) and the quantification of percent and absolute number (right) of neutrophils in the lung tissues of *Mapk14*$^{fl/fl}$ and *Mapk14*$^{\Delta Fib}$ mice pretreated with SFM, B16F10 TCM, MH6499c4 TCM followed by intravenous injection of 5*10^{5} B16F10-TdTomato cells. Quantitative data shown as mean ± SEM (n = 4 mice for SFM treated group, n = 5 mice for TCM treated group). Two-way ANOVA and Tukey's multiple comparisons test were performed. **f**, Representative flow cytometry analysis of tumor cells (TdTomato^{+}) in the lung tissues of *Mapk14*$^{fl/fl}$ and *Mapk14*$^{\Delta Fib}$ mice pretreated with SFM, B16F10 TCM, or MH6499c4 TCM followed by intravenous injection of 5*10^{5} B16F10-TdTomato cells. The experiments in **a**, **b**, **c**, **f** were repeated three times independently with similar results, and the results of one representative experiment are shown.

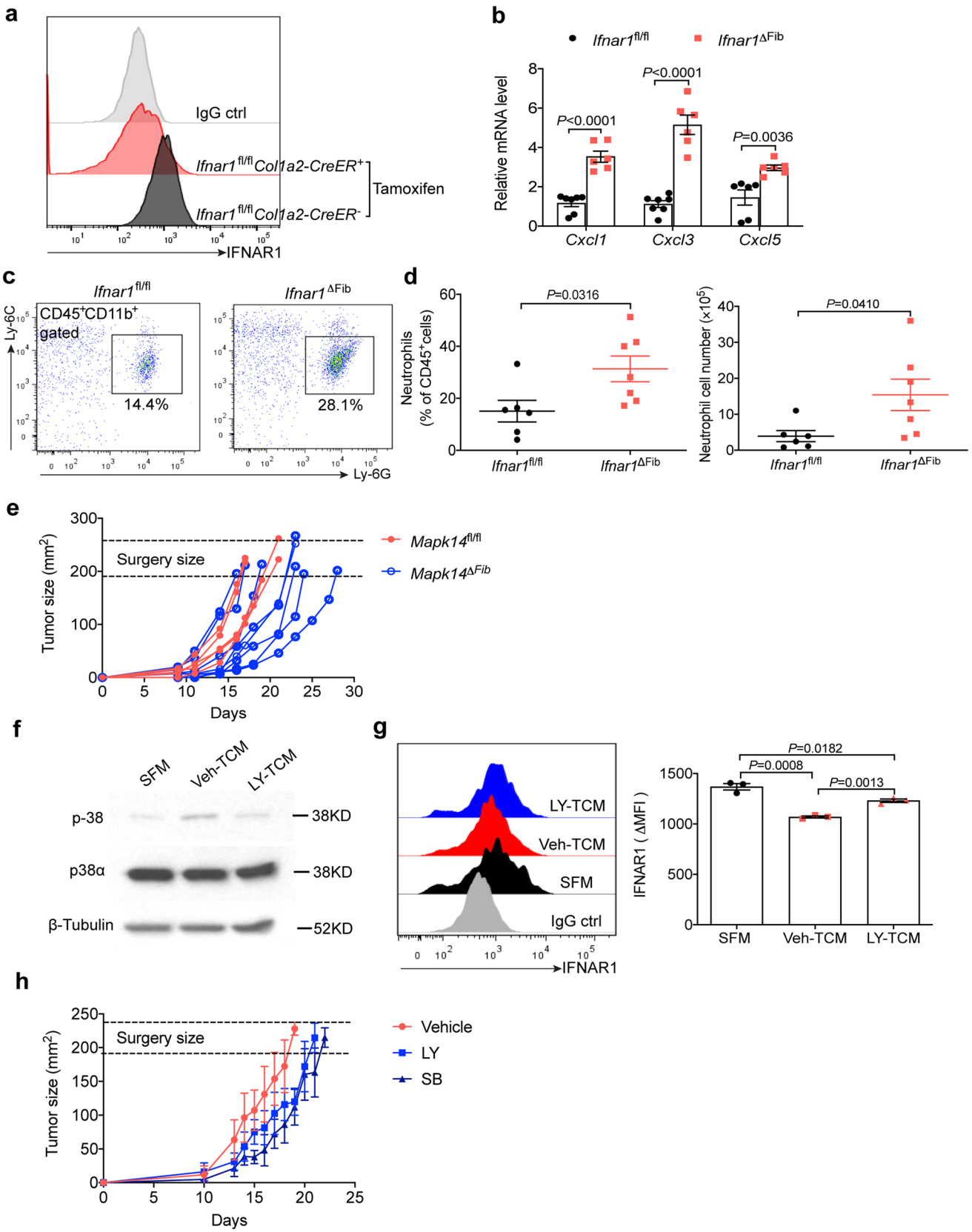

Extended Data Fig. 8 | See next page for caption.

Extended Data Fig. 8 | The effect of p38α deficiency specifically in fibroblasts and p38 inhibitors on the primary tumor. a, Representative flow cytometry analysis of IFNAR1 level in the isolated lung fibroblasts from tamoxifen treated *Ifnar1*$^{fl/fl}$*Col1a2-CreER*$^{-}$ (*Ifnar1*$^{fl/fl}$) and *Ifnar1*$^{fl/fl}$*Col1a2-CreER*$^{+}$ (*Ifnar1*$^{\Delta Fib}$, *Ifnar1* knock out specific in fibroblasts*)* mice. Similar results were obtained from three independent experiments. **b**, qPCR analysis of the indicated chemokines in the lung tissues of *Ifnar1*$^{fl/fl}$ (n = 7 mice) and *Ifnar1*$^{\Delta Fib}$ mice (n = 6 mice) after intravenous injection with 5*10^{5} B16F10-TdTomato cells. Data shown as mean ± SEM. Two-way ANOVA and Sidak's multiple comparisons test were performed. **c**, Representative flow cytometry analysis of neutrophils in the lung tissues of *Ifnar1*$^{fl/fl}$ and *Ifnar1*$^{\Delta Fib}$ mice after intravenous injection with 5*10^{5} B16F10-TdTomato cells. Similar results were obtained from three independent experiments. **d**, Quantification of the percent (left) and the absolute number of neutrophils (right) in the lung tissues as described in **c**. Data shown as mean ± SEM (n = 6 mice for *Ifnar1*$^{fl/fl}$ group, n = 7 for *Ifnar1*$^{\Delta Fib}$ group). Two-tailed Unpaired t test was performed for the comparison. **e**, The primary tumor growth of B16F10 in the *Mapk14*$^{fl/fl}$ (n = 5 mice) and *Mapk14*$^{\Delta Fib}$ (n = 8 mice) mice s.c injected with 1×10^{5} B16F10 tumor cells prior to surgery at equivalent tumor size (~200 mm^{2}). **f**, A representative western blot analysis of p-p38 and total p38 in the WT lung fibroblasts 1 hr after treatment with SFM, or TCM from B16F10 tumor cells pretreated with vehicle (DMSO) or p38 inhibitor LY2228820 (4 μM) for 24 hr. Similar results were obtained from three independent experiments. **g**, A representative flow cytometry histogram (left) and the quantification of surface IFNAR1 level (right) in WT lung fibroblasts 2 hr after treatment with SFM, or TCM from B16F10 tumor cells pretreated with vehicle (DMSO) or p38 inhibitor LY2228820 (4 μM) for 24 hr. Quantitative data shown as mean ± SEM (n = 3 biologically independent samples). Two- tailed Unpaired t test was performed for the comparisons between two groups. **h**, Primary tumor growth of B16F10 in mice that received vehicle, LY2228820 (LY), or SB203580 (SB) treatment prior to surgery at equivalent tumor size (~200 mm^{2}). Data shown as mean ± SEM (n = 6 mice per group).

nature research

Corresponding author(s): Serge Y. Fuchs

Last updated by author(s): 3/18/2020

Reporting Summary

Nature Research wishes to improve the reproducibility of the work that we publish. This form provides structure for consistency and transparency in reporting. For further information on Nature Research policies, see Authors & Referees and the Editorial Policy Checklist.

Statistics

For all statistical analyses, confirm that the following items are present in the figure legend, table legend, main text, or Methods section.

n/a	Confirmed	
☐	☒	The exact sample size (*n*) for each experimental group/condition, given as a discrete number and unit of measurement
☐	☒	A statement on whether measurements were taken from distinct samples or whether the same sample was measured repeatedly
☐	☒	The statistical test(s) used AND whether they are one- or two-sided *Only common tests should be described solely by name; describe more complex techniques in the Methods section.*
☒	☐	A description of all covariates tested
☐	☒	A description of any assumptions or corrections, such as tests of normality and adjustment for multiple comparisons
☐	☒	A full description of the statistical parameters including central tendency (e.g. means) or other basic estimates (e.g. regression coefficient) AND variation (e.g. standard deviation) or associated estimates of uncertainty (e.g. confidence intervals)
☐	☒	For null hypothesis testing, the test statistic (e.g. *F*, *t*, *r*) with confidence intervals, effect sizes, degrees of freedom and *P* value noted *Give P values as exact values whenever suitable.*
☒	☐	For Bayesian analysis, information on the choice of priors and Markov chain Monte Carlo settings
☒	☐	For hierarchical and complex designs, identification of the appropriate level for tests and full reporting of outcomes
☒	☐	Estimates of effect sizes (e.g. Cohen's *d*, Pearson's *r*), indicating how they were calculated

Our web collection on statistics for biologists contains articles on many of the points above.

Software and code

Policy information about availability of computer code

Data collection	QuantStudioTM Real-time PCR Software v1.3 was used to collect Real-time PCR data. Leica Application Suite X Software 3.3.0.16799 was used to acquire histological image. Illumina BeadStudio 3.1.1.0 software was used to collect microarray data. BD FACSDiva software 8.0.1 was used to collect flow cytometry data. SPOT Advanced software 2.0 was used to collect Fluorescent image.
Data analysis	Image J 1.51 n was used to analyze the fluorescent images and histological images. FlowJo v10.0 was used to analyze FACS data. GraphPad Prism 8 was used to perform statistical analysis.

For manuscripts utilizing custom algorithms or software that are central to the research but not yet described in published literature, software must be made available to editors/reviewers. We strongly encourage code deposition in a community repository (e.g. GitHub). See the Nature Research guidelines for submitting code & software for further information.

Data

Policy information about availability of data

All manuscripts must include a data availability statement. This statement should provide the following information, where applicable:

- Accession codes, unique identifiers, or web links for publicly available datasets
- A list of figures that have associated raw data
- A description of any restrictions on data availability

RNA-sequencing data that support the findings of this study have been deposited in the Gene Expression Omnibus (GEO) under accession code GSE133781. Source data for Figs. 1–8 and Extended Data Figs. 1–8 have been provided as Source Data files. All other data supporting the findings of this study are available from the corresponding author upon reasonable request.

Field-specific reporting

Please select the one below that is the best fit for your research. If you are not sure, read the appropriate sections before making your selection.

☒ Life sciences ☐ Behavioural & social sciences ☐ Ecological, evolutionary & environmental sciences

For a reference copy of the document with all sections, see nature.com/documents/nr-reporting-summary-flat.pdf

Life sciences study design

All studies must disclose on these points even when the disclosure is negative.

Sample size	Sample sized were determined according to the basis of previous published studies. Generally more than 4-6 mice per group were used to ensure the statistically significance could be obtained. No statistical method was used to predetermine sample size.
Data exclusions	Mice that died within 24 h after surgery were assumed to have died because of procedure-related complications and were excluded from analysis. In Western blot analysis of human blood leukocytes, three samples were excluded due to the too low amount of protein (<1 ug) which was less than the minimal amount of protein required for Western blot. No other data exclusions were made. No exclusion criteria were pre-established.
Replication	All described results are representative of at least three independent experiments. Results of animal experiments are based on representative results of 3 independent cohorts of mice following the same protocol. All findings were replicated successfully.
Randomization	Experimental mice were randomly assigned into the experimental groups
Blinding	Investigators were not blinded to allocation during the experiments and outcome assessment except for the IHC score analysis.

Reporting for specific materials, systems and methods

We require information from authors about some types of materials, experimental systems and methods used in many studies. Here, indicate whether each material, system or method listed is relevant to your study. If you are not sure if a list item applies to your research, read the appropriate section before selecting a response.

Materials & experimental systems

n/a	Involved in the study
☐	☒ Antibodies
☐	☒ Eukaryotic cell lines
☒	☐ Palaeontology
☐	☒ Animals and other organisms
☐	☒ Human research participants
☒	☐ Clinical data

Methods

n/a	Involved in the study
☒	☐ ChIP-seq
☐	☒ Flow cytometry
☒	☐ MRI-based neuroimaging

Antibodies

Antibodies used

Biolegend: anti-mouse CD16/CD32(Clone 93; Cat# 101302, Lot# B264872, 1:50), anti-mouse CD45-FITC (Clone 30-F11; Cat# 103108, Lot# B17644, 1:500), anti-mouse/human CD11b-APC (Clone M1/70, Cat# 101212, Lot# B261578, 1:500), Anti-mouse Ly-6C-PE (Clone HK1.4, Cat# 128007, Lot# B17063, 1:500), Anti-Ly-6G-APC/Cy7 (Clone 1A8, Cat# 127624, Lot# B175206, 1:500), Anti-mouse IFNAR1-PE (Clone MAR1-5A3, Cat# 127312, Lot# B251510, 1:500), mouse IgG1 isotype control (Clone MOPC-21, Cat# 400112, Lot# B291605, 1:500), Rat anti-mouse CD11b (Clone M1/70, Cat# 101202, Lot# B261558, 1:100), Rat IgG1 isotype control (Clone G0114F7, Cat# 401902, Lot# B219991, 1:100), Anti-mouse CD45-APC/Cy7(Clone 30-F11, Cat#103115, Lot# B257633, 1:500), Anti-mouse CD31-AF488 (Clone MEC13.3, Cat#102513, Lot# B191233, 1:500), Anti-mouse EpCAM-PE/Cy7 (Clone G8.8, Cat#118216, Lot# B210354, 1:500), Anti-mouse CD140a-APC (Clone APA5, Cat# 135908, Lot# B221113, 1:500).
Santa Cruze: anti p38α (Clone C-20, Cat#sc-535, Lot#D01914, 1:1000).
Cell Signaling Technology: anti-phospho-p38 (Clone 28B10; Cat# 9216S, Lot# 27, 1:1000), GAPDH (Clone D16H11; Cat# 5174S, Lot# 8, 1:5000), β-Tubulin (Cat# 2146S, Lot# 7, 1:5000). Goat anti-mouse HRP IgG (Cat#7076S, Lot# 29, 1: 20000).
Millipore: Goat anti-rabbit HRP IgG (Cat#AP187P, small aliquot, Lot# could not be found, 1:20000)
Abcam: anti-Fibronectin (Cat# ab23750, Lot# GR3225982-1, 1:100), anti-H3K4me3 (Cat# ab8580, Lot# GR3207339-1, 1 µg/ml), anti-H3K9me3 (Cat# ab8898, Lot# GR3217826-1, 1 µg/ml), isotype control (Cat# ab171870, Lot# GR3228514-3, 1 µg/ml).
Sino Biological Inc.: anti-mouse IFNAR1 (Cat# 50469-RP02, Lot# HB04OC2703-B, 1:100)
R&D systems: anti-FAP (Cat# AF3715, Lot# ZKW0315081, 1:100), Sheep IgG isotype control (Cat# 5-001-A, Lot# WAX041411, 1:100)
Thermo Fisher Scientific: Alexa Fluor 488 Donkey anti-sheep (Cat# A11015, Lot# 2079356, 1:500), Alexa Fluor 488 Goat anti-Rabbit (Cat# A11070, Lot# 2119159, 1:500), Alexa Fluor 488 Goat anti-Rat (Cat# A11006, Lot# 1156624, 1:500), Alexa Fluor 594 Goat anti-Rabbit (Cat# A11072, Lot# 1866858, 1:500)

Validation	Validation for all the antibodies can be found on the respective datasheets for each antibody on the manufacturer's websites.

Eukaryotic cell lines

Policy information about cell lines

Cell line source(s)	Mouse melanoma cell lines B16F1 (ATCC® CRL-6323™) and B16F10 (ATCC® CRL-6475™) were purchased from ATCC. Mouse mammary adenocarcinoma cell line E0771 was purchased from CH3 Biosystems (Cat#940001). Mouse pancreatic tumor cell clone MH6499c4 was isolated from late-stage primary tumors from a spontaneous tumor model provided by Ben Z. Stanger lab (University of Pennsylvania). HEK293 T cells were kindly provided by Dr. Warren S. Pear (University of Pennsylvania). MC38 colon adenocarcinoma cells were provided by S. Ostrand-Rosenberg (University of Maryland)
Authentication	None of the cell lines were authenticated.
Mycoplasma contamination	The cell lines tested negative for mycoplasma.
Commonly misidentified lines (See ICLAC register)	No commonly misidentified lines were used.

Animals and other organisms

Policy information about studies involving animals; ARRIVE guidelines recommended for reporting animal research

Laboratory animals	Littermates Ifnar1+/+ (''WT'') and Ifnar1S526A mice (''SA'') were maintained by our lab. Fap-/- mice were from Dr. Ellen Pure lab. Ifnar1-/- mice were generously provided by Dr. Susan Weiss and maintained by our lab. Ubc9-CreER mice (gift from E. Brown, University of Pennsylvania) were crossed with Mapk14fl/fl mice (generously provided by Yibin Wang, University of California, Los Angeles) and either Ifnar1-/- mice to generate Ubc9-CreER+/0; Mapk14fl/fl; Ifnar1+/+ or Ubc9-CreER+/0; Mapk14fl/fl;Ifnar1-/- littermates. Col1a2-CreER mice (obtained from Jackson Laboratory) were crossed with Mapk14fl/fl mice or Ifnar1fl/fl mice (obtained from Jackson Laboratory) to generate Col1a2-CreER+/0; Mapk14fl/fl or Col1a2-CreER+/0; Ifnar1fl/fl littermates respectively. All these mice were C57/Bl6 background. Experiments were performed with gender matched-young adults (6-8 weeks old, either male or female, but the same gender in one cohort for each independent experiment). FapS624A knock-in mice expressing FAP mutant were generated by Tak W. Mak lab and backcrossed with WT C57Bl/6 mice in Dr. Ellen Pure lab. The homozygotes (mixed background of 129/Sv and C57Bl/6) were used only for lung fibroblasts isolation.
Wild animals	The study did not involve wild animals.
Field-collected samples	The study did not involve field-collected samples.
Ethics oversight	Animal protocol 803995 was approved by the Institutional Animal Care and Use Committee (IACUC) of The University of Pennsylvania.

Note that full information on the approval of the study protocol must also be provided in the manuscript.

Human research participants

Policy information about studies involving human research participants

Population characteristics	Patients with melanoma were diagnosed at different stages (stage I, II, III or IV). They were 54.35±17.48 years old.
Recruitment	Subjects were recruited through Medical Center in the University of Pittsburgh. Peripheral blood was drawn when the patients got diagnosed. Recruitment was based solely on sample availability. No patient characteristic related bias is likely to be present.
Ethics oversight	Informed consent was obtained from all study participants. Study approval was given by the Institutional Review Board of the University of Pittsburgh.

Note that full information on the approval of the study protocol must also be provided in the manuscript.

Flow Cytometry

Plots

Confirm that:

☒ The axis labels state the marker and fluorochrome used (e.g. CD4-FITC).

☒ The axis scales are clearly visible. Include numbers along axes only for bottom left plot of group (a 'group' is an analysis of identical markers).

☒ All plots are contour plots with outliers or pseudocolor plots.

☒ A numerical value for number of cells or percentage (with statistics) is provided.

Methodology

Sample preparation	Lung tissues were collected and washed with ice cold PBS, and then cut into small pieces, and incubated in dissociation solution with 2 mg/ml Collagenase II, 1 mg/ml Collagenase IV plus 100 µg/ml Dnase I solution for around 1 hr with continuous agitation. Digestion mixture was passed through 70 µm cell strainer and washed with PBS for one time. 5 ml RBC lysis buffer was added into cells and incubated for 5 mins to lysis red blood cells. The cells were washed with PBS for one time and re-suspended with 1% BSA-PBS contained 1 mM EDTA. The isolated cells were incubated with anti-mouse CD16/CD32 antibody for 15 mins at room temperature to block non-specific Fc receptor binding. Cells were then stained with cell surface markers. For IFNAR1 and FAP staining on the lung fibroblasts in vitro, cells were incubated with cell dissociation buffer for 15 mins and dispersed into single-cell suspension. After washing with PBS, cells were stained with PE conjugated anti-mouse IFNAR1 for 30 mins, or biotinylated anti-mouse FAP for 30 mins followed by a secondary streptavidin-APC staining for another 30 mins. Cells stained with PE conjugated IgG-ctrl or only secondary staining was as negative control. After washing, cells were re-suspended with FACS buffer contained with DAPI for 10 mins.
Instrument	Data were collected by BD LSRFortessa.
Software	BD FACS Diva was used to used to acquire data and FlowJo (Tree Star) was used for analysis.
Cell population abundance	In most cases, cell populations are calculated as %CD45+ Live cells.
Gating strategy	For neutrophils gating, cells gated from the SSC-A/FSC-A plot were then plotted on FSC-H/FSC-A and single cells were gated. These cells were plotted against the cell viability marker (DAPI) and negative cells were selected. These cells were plotted on FSC-A/CD45and CD45 positive cells were selected. These cells were plotted on FSC-A/CD11b and CD11b positive cells were selected. These cells were plotted on Ly-6C/Ly-6G and Ly-6G positive/Ly-6C low expression cells were gated. For IFNAR1 staining in gated lung fibroblasts in vivo, cells cells gated from the SSC-A/FSC-A plot were then plotted on FSC-H/FSC-A and single cells were gated. These cells were plotted against the cell viability marker (DAPI) and negative cells were selected. These cells were plotted on FSC-A/CD45and CD45 negative cells were selected. These cells were plotted on FSC-A/CD31 and CD31 negative cells were selected. These cells were plotted on EpCAM/CD140a(PDGFRa) and EpCAM negative CD140a positive cells were gated. A histogram of the IFNAR1 yield the MFI for that marker in this population. For the IFNAR1 or FAP staining in the lung fibroblasts, cells gated from the SSC-A/FSC-A plot were then plotted on FSC-H/FSC-A and single cells were gated. These cells were plotted against the cell viability marker (DAPI) and negative cells were selected. A histogram of the marker yield the MFI for that marker in this population.

☐ Tick this box to confirm that a figure exemplifying the gating strategy is provided in the Supplementary Information.